RSC Sustainability

ROYAL SOCIETY OF CHEMISTRY

PAPER

View Article Online
View Journal | View Issue

Cite this: *RSC Sustainability*, 2025, **3**, 5367

Green conversion of a soft commodity into visible light-activated N–S doped carbon quantum dots with antibacterial properties

Yohanz Khor,[a] Su Sin Chong,[*a] A. R. Abdul Aziz,[b] Ching Shya Lee[c] and Eugene Ling Wei Hong[a]

Carbon quantum dots (CQDs), with particle sizes less than 10 nm, have been introduced as a promising alternative for water antimicrobial applications. In this study, the authors proposed an effective, green, and sustainable method for producing nature-based nitrogen–sulphur-doped carbon quantum dots (N–S-CQDs) from sugar and onion through a one-step microwave reaction carbonization process. Results showed that N–S-CQDs processed optimally with a 7 : 3 ratio of sugar and onion, at a pH of 7–8, microwave power of 850 W, and a synthesis time of three minutes, exhibited the best fluorescence characteristics. The synthesized sample exhibited excitation within the visible region, with particle sizes of 4 to 6 nm, and amorphous characteristics. Cytotoxicity tests were performed using HeLa cells, with tetracycline as a positive control. Results indicated that the test material exhibits a non-significant cytotoxic effect on HeLa cells, with an IC50 value below 58 mg mL^{-1}. This cytotoxic effect is relatively low compared to that of carbon dots, which caused significant toxicity at 2 mg mL^{-1}. Zeta potential test demonstrated good stability of electrical charge on the surface of N–S-CQDs. According to SEM results, N–S-CQDs caused bacterial cell surface destruction, likely due to changes in the charge balance of the bacterial surface, leading to membrane disruption in both Gram-negative *E. coli* and Gram-positive *S. aureus* strains. A promising antibacterial effect was observed in Gram-negative *E. coli* strains, comparable to those of commercial antibiotics like tetracycline. For further verification of the antimicrobial effect, Gram-negative bacteria such as *Salmonella typhimurium* and *Vibrio parahaemolyticus* were tested, showing significant zones of inhibition at concentrations of 125 mg mL^{-1}, 250 mg mL^{-1}, and 500 mg mL^{-1}.

Received 9th February 2025
Accepted 23rd September 2025

DOI: 10.1039/d5su00087d

rsc.li/rscsus

Sustainability spotlight

This study addresses the urgent need for sustainable antimicrobial solutions in water treatment, which is a critical concern as antibiotic resistance and waterborne pathogens are increasingly threatening the global health. A green, low-toxicity method is developed to synthesize nitrogen–sulphur-doped carbon quantum dots using natural precursors—sugar and onion—through a rapid, energy-efficient microwave carbonization process. The conversion method significantly reduces the environmental impact by eliminating harsh chemicals and energy-intensive synthesis. The prepared carbon quantum dots demonstrate strong antibacterial efficacy against both Gram-negative and Gram-positive bacteria, with notably low cytotoxicity compared with conventional carbon dots. This work aligns with several UN Sustainable Development Goals (SDGs), including SDG 3 (good health and well-being) and SDG 12 (responsible consumption and production), by advancing eco-friendly technologies that support public health and environmental sustainability.

Introduction

In recent years, the emergence of drug-resistant bacteria has been worsening the threat of bacterial infections worldwide, causing the infections to be more problematic to cure.[1,2] Bacteria such as *Escherichia coli* (*E. coli*) and *Staphylococcus aureus* (*S. aureus*) have been reported to have evolved resistance mechanisms towards almost all antibacterial drugs,[3,4] thus posing a major challenge in preparing alternative antimicrobial agents that have high antibacterial properties, especially for bacteria-infected wound healing purposes. In recent years, the emergence of nanotechnology has contributed to the creation of non-antibiotic bactericides. Noble metal nanoparticles, such as Au, Ag, Pd, Ru, and Pt,[5–10] and metallic oxide nanoparticles, such as ZnO, TiO_2, and CuO,[11–13] have been developed as antibacterial substitutes due to their great bacterial cell viability

[a]*School of Energy and Chemical Engineering, Xiamen University Malaysia, Selangor Darul Ehsan, Malaysia. E-mail: susin.chong@xmu.edu.my*

[b]*Department of Chemical Engineering, Faculty of Engineering, University of Malaya, 50603 Kuala Lumpur, Malaysia*

[c]*Nanotechnology & Catalysis Research Centre, University of Malaya, Advanced Studies Complex, 50603 Kuala Lumpur, Malaysia*

inhibition. However, there are limitations, such as high costs, biosafety concerns, and complex synthesis, and their production is not viable to exceed laboratory scale. Carbon-based nanomaterials, such as carbon quantum dots (CQDs), graphene, and graphene oxide, have also been established to exhibit excellent antibacterial properties and biocompatibility.[14,15] Hence, they are considered a better choice as antibacterial agents.

CQDs are a new class of quantum dots (QDs) that have attracted attention as fluorescent nanoparticles utilised in multiple applications.

Differing from their predecessors (QDs), CQDs are 0D carbon nanoparticles, with sizes below 10 nm and 0.34 nm lattice parameter corresponding to the graphite (002) *d*-spacing, and they are often extracted from natural resources such as lemons and oranges.[16] Furthermore, any carbohydrate can be used to synthesize CQDs if and only if the C, H, O ratio is 1 : 2 : 1.[17] Therefore, CQDs are commonly known for being non-toxic and safe for humans. Moreover, CQDs can be functionalized with various surface functional groups, resulting in CQDs with different excellent properties. For example, the oxygen-containing functional groups (hydroxyl, epoxy, carbonyl, carboxyl) on the surface of a CQD core resulted in the solubility of CQDs and stable colloid formation in aqueous and polar organic solvents.[18] Surface functional groups also provide a simple functionalization platform with different species.[16] In addition, the surface functional groups of CQDs improve their biocompatibility, targeting ability, and optical properties. Properties such as their high water solubility and biocompatibility prove that CQDs have the potential to be applied in various fields, including drug delivery, gene delivery, and phototherapy.[18]

CQDs exhibit normal photoluminescence or down-converted photoluminescence, similar to QDs. Nevertheless, CQDs can also exhibit up-converted photoluminescence, which is favourable for applications like photodynamic therapy.[19] Furthermore, the photoluminescence in CQDs ranges from the deep ultraviolet to near-infrared regions (200–800 nm). This could be tuned by altering the size, shape, edges, and surface, and doping with heteroatoms due to the quantum confinement effect (QCE), surface effect, and edge effect.[16] In addition, unlike most of the QDs and organic dyes, CQDs are photo-stable and resistant to photobleaching and blinking.[20] Differing from QDs that can tune the bandgap and fluorescence *via* the application of QCE, which alters the particle size, the fluorescence of CQDs occurs due to the radiative recombination of holes and electrons, and thus QCE could not be applied to CQDs.[16] The size-dependent optical properties of CQDs may be caused by the various surface defect sites and surface-to-volume ratio of the dots.[21] Despite CQDs seemingly being advantageous over QDs, CQDs obtained from natural resources have been reported to exhibit lower emission and quantum yields. Therefore, green precursors could be used to enhance performance. As an example, based on the research by Bandi *et al.*, onion biowastes are found to successfully produce CQDs of high fluorescence quantum yield (28%) due to their high nitrogen content and *in situ* surface passivation by the formation of amide bonds.[22]

Identical to graphene quantum dots (GQDs), CQDs are famous for their core–shell structure. Nevertheless, both GQDs and CQDs are significantly different in their chemical structures. For GQD, the core consists of one or multiple layers of graphene and is connected to chemical groups on the edge, which form the shell.[23] On the other hand, the structure of the CQDs is a combination of defect states, which is an sp^3-hybridized matrix of surface functional groups, and the intrinsic states, which form the core.[24] CQDs are formed due to a nucleation process with a gradually growing core and a "self-passivated" shell.[25] Previous studies have proved that the electronic acceptor levels and optical properties are related to both the core and shell of the CQDs, whereas the hydrogen bonding behaviour is manipulated by the chemical nature of the shell.[25]

The surface chemistry of the shell of the CQDs includes the chemical structure and the functions. In terms of chemical structure, there are multiple functional groups in the CQD shell, which depend on the synthesis materials or dopants.[26] On the other hand, in terms of functions, the shell surface chemistry manipulates the CQDs' stability in aqueous solution. The lower the zeta potential value of the surface, the weaker the electrostatic repulsion among the CQDs, thus the lower the stability of the CQDs in aqueous solution.[27] Moreover, the CQDs' shell is also responsible for the extraordinary optical properties, as well as the electron acceptor or donor behaviour of the CQDs. As an example, studies have proved that CQDs possess pH-dependent photoluminescence, where the effects of the surface functional groups on the optical properties have been studied by monitoring the photoluminescence at different pH.[28] Furthermore, the surface moieties can also modulate the surface electronic acceptor levels, thus affecting the photoluminescence of the CQDs. Therefore, surface passivation and functionalization are crucial since the surface character of CQDs is thought to be substantially responsible for the fluorescence emitted.

Despite CQDs being theoretically able to replace the highly toxic QDs in the near future, most high-yield CQDs are still synthesized with the aid of chemicals. For example, CQDs of 28% yield synthesized by Bandi *et al.* utilised ethylene diamine (EDA) as one of the precursors.[22] Although studies have shown that CQDs synthesized with chemicals have low toxicity, these studies have yet to show the impact of CQDs on the human body, especially when exposed multiple times. Therefore, in terms of applications where the human body could potentially be exposed to CQDs, it would be preferable for the products used to be of zero toxicity. This includes *in vivo* applications such as bioimaging and nanomedicines, as well as *in vitro* applications such as water monitoring.

Despite the successful synthesis of high-yield CQDs in multiple studies,[22,29–31] the use of toxic chemicals in the synthesis procedure is still a major limitation for the utilisation of CQDs in applications associated with human exposure or health. Furthermore, some studies have shown that the synthesis procedure is time-consuming, which is not beneficial on an industrial scale because it leads to a high cost of synthesis. Moreover, most studies have shown that the synthesized CQDs exhibited excitation maxima in the UV region, which is not feasible for applications that involve human

exposure. The requirement of UV light for CQDs to exhibit emission is unsafe since overexposure to UV radiation could cause cancer.

Hence, research into nature-based CQDs is important and has attracted significant attention recently due to their zero-toxicity and degradable by-products. Despite the multiple advantages, nature-based CQDs have a disconcerting disadvantage, which is the exhibition of lower yields in comparison to chemical-based CQDs.[32] To overcome the low yield limitation, studies on the doping of heteroatoms onto CQDs have been conducted over the years. CQDs have variable surface states that correspond to the different energy levels they emit to construct broad and excitation-dependent emission spectra, as well as a broad UV-visible absorption band.[33] To enhance the fluorescence properties, increase quantum yields, as well as achieve tuneable chemical and electronic properties, CQDs have been doped with heteroatoms such as nitrogen and sulphur. Due to the surface passivation by heteroatoms, the surface defects act as excitation energy traps and affect the photoluminescence of the CQDs.[34] In this study, one of the heteroatoms, the sulphur atom, functions as a catalyst for the oxidation–reduction reaction, which increases the passivated surface defects of the CQDs, thus increasing the photoluminescence.[35] Besides that, the doping of nitrogen atoms forms the N-state, a new kind of surface state where trapped electrons could be utilised to promote radiative recombination with high yield.[36] This was shown when Duan *et al.* synthesized N–S-doped CQDs using ethylenediamine as the carbon source and sulfamic acid as the surface passivation agent, which resulted in 28% quantum yield.[37]

Nevertheless, recent studies have yet to successfully synthesize naturally based doped CQDs. Most studies are still heavily focused on the use of chemicals to produce doped CQDs, including N-doped CQDs,[38] S-doped CQDs,[38,39] P-doped CQDs,[40] as well as hybrid-doped CQDs.[37,41] Although the produced CQDs are of high yield, they are still not feasible for applications involving human consumption and exposure to the body due to the use of toxic chemicals for synthesis. Therefore, instead of using chemicals as the main synthesis materials, doped CQDs should be synthesized from natural resources to produce non-toxic, high-yield CQDs for safe utilisation by consumers.

Furthermore, some studies have shown that the synthesis procedure is time-consuming, which is not beneficial on an industrial scale because it leads to a high cost of synthesis. Hence, to favour the purpose of commercialization, CQDs that could be synthesized in a short amount of time, as well as requiring low synthesis costs, will be very beneficial. The cheap, fast, and simple synthesis of the CQDs is very favourable towards large-scale industries as it vastly reduces the production cost and manpower, thus aiding in the commercialization of the CQDs. Therefore, in this study, green and less time-consuming methods have been explored to solve this limitation.

CQDs have also been established to exhibit excellent antibacterial properties and biocompatibility. To combat the emergence of drug-resistant bacteria, CQDs have been studied to create a better and safer substitute for antibacterial applications. Despite this being so, few studies have reported the antibacterial activity of nature-based CQDs. Roy *et al.* studied CQDs synthesized from resorcinol and formaldehyde resins, which resulted in good antibacterial activity.[42] Travlou *et al.* also reported significant antibacterial activity of both N-doped CQDs derived from polyvinylpyrrolidone and S-doped CQDs derived from poly(sodium-4-styrene sulfonate).[38] Chai *et al.* also derived P-doped CQDs from *m*-aminophenol and phosphoric acid, which showed effective antibacterial activity.[40] In addition, some studies showed that CQDs require the addition of H_2O_2 and light irradiation to form reactive oxygen species (ROS) and promote antibacterial activity.[22–24] Table 1 shows a summary of previous studies of CQDs in antibacterial applications. Based on Table 1, it was found that the CQDs synthesized from previous studies for antibacterial applications are chemical-based, which drastically limited their application in water quality control due to the risk of harmful chemicals intoxicating the consumable water. Although most studies perform cytotoxicity analysis on the CQDs synthesized, the concentration tested was very low, which is impractical for large-scale applications due to the unknown risk at high concentrations.

Furthermore, some studies do not provide a detailed evaluation of the antibacterial mechanism behind the CQDs. Although CQDs are known to exhibit antibacterial properties, many factors could influence the inhibition result, such as surface charge and surface functional groups. Hence, the antibacterial mechanism involved by the CQDs should be evaluated in detail to prove that the CQDs are the main reason for the inhibition.

Most previous studies have performed inhibition on only one bacterial species for both Gram-positive and Gram-negative bacteria. However, this could only prove their inhibition towards the specific bacterial species and not the whole bacterial group. Pandiyan *et al.*[43] proved that the CQDs synthesized in their studies exhibited inhibition of various Gram-positive and Gram-negative bacteria, thus indirectly proving that the CQDs synthesized exhibited inhibition of both bacteria groups. In addition, most previous studies do not perform time-dependent inhibition analysis, which can indirectly prove the stability of the antibacterial capabilities of the CQDs. Chai *et al.*[40] reported that the CQDs synthesized in their study showed long-term inhibition at high concentration, which is beneficial for commercialization against conventional antibiotics, which mostly exhibit inhibition for 8 to 12 hours.

One of the most encouraging approaches in combating MDR pathogens involves utilizing the photodynamic inactivation of bacteria facilitated by photosensitizers. This approach is dependent on the light-induced creation of highly reactive oxygen species (ROS) capable of deactivating bacterial cells through various mechanisms, such as damaging membranes and causing irreversible harm to proteins and DNA.[48–50] A fundamental aspect of photodynamic therapies is the establishment of a localized physicochemical environment that is detrimental to bacterial cells, achieved through ROS generation or elevation in temperature (referred to as photothermal (PTT) effects), which poses challenges for developing resistance.[51,52] Within the array of photosensitizers available, carbon dots (CDs) have emerged as a promising category of nanomaterials

Table 1 Summarized conditions, results, and limitations of CQDs in antibacterial applications

CQD condition		Bacteria tested				
Precursors	Heteroatom doping	Gram-positive	Gram-negative	Antibacterial results	Limitations	References
Poly (sodium-4-styrene sulfonate)	S-doped	*B. subtilis*	*E. coli*	-Very effective towards Gram-positive -Less effective towards Gram-negative	-Use of toxic chemicals as precursors -No cytotoxicity analysis performed	38
Polyvinylpyrrolidone	N-doped	*B. subtilis*	*E. coli*	-Very effective towards Gram-positive -Less effective towards Gram-negative	-Use of toxic chemicals as precursors -No cytotoxicity analysis performed	38
m-Aminophenol and phosphoric acid	P-doped	*S. aureus*	*E. coli*	Slightly more effective towards Gram-negative (1.23 mg mL^{-1}) than Gram-positive (1.44 mg mL^{-1})	-Use of toxic chemicals as precursors -No discussion on the antibacterial mechanism of CQDs -Cytotoxicity analysis was performed at a maximum of 0.5 mg mL^{-1}	40
Resorcinol and formaldehyde	—	*S. aureus*	*E. coli*	Clear inhibition zones were observed for both bacterial groups	-Use of toxic chemicals as precursors -Cytotoxicity analysis was performed at a maximum of 0.1 mg mL^{-1} -No detailed analysis on the antibacterial capabilities of CQDs -No discussion on the antibacterial mechanism of CQDs	42
Sugarcane bagasse pulp, citric acid, and aqueous ammonia	—	*B. cereus S. aureus*	*P. aeruginosa V. cholera E. coli*	Most effective towards *B. cereus*, and overall, more effective towards Gram-positive bacteria than Gram-negative bacteria	-Use of toxic chemicals as precursors -No evaluation on the antibacterial mechanism of CQDs -No cytotoxicity analysis performed	43
Polyoxyethylene-polyoxypropylene-polyoxyethylene Pluronic 68, phosphoric acid, and toluene	—	*S. aureus*	*E. coli*	More effective towards *E. coli* than *S. aureus* when exposed to blue light. After exposure to gamma irradiation, the inhibition efficiency for both bacteria significantly increased	-Use of toxic chemicals as precursors -Cytotoxicity analysis was performed without detailed concentration values -Gamma radiation is required for efficient inhibition of bacteria	44
Figs of *Ficus religiosa* tree		*B. subtilis*	*E. coli*	Exhibited bactericidal activity against both bacterial strains	- No cytotoxicity analysis performed	45
Psidium guajava L. leaves, manganese sulfate monohydrate	Mn-doped	—	*E. coli*	Under white light, the C-dots showed the best antibacterial activity against ampicillin-resistant green fluorescence protein (GFP)-expressing recombinant *E. coli*	- No cytotoxicity analysis performed - Use of toxic chemicals as precursors	46
Joshina (Plant-derived biomass), zinc sulfate heptahydrate	Zn-doped (metal)	*S. aureus*	*S. marcescens*	Bactericidal effect was exhibited against both strains, where a stronger effect was seen against the Gram-negative strain	- No cytotoxicity analysis performed - Use of toxic chemicals as precursors	47

for the precise identification and deactivation of diverse bacterial strains.[53,54] Carbon dots (CDs) constitute a category of quasi-spherical, carbon-based fluorescent materials. Previous studies have confirmed that the functional groups on the surface of carbon quantum dots (CQDs) are also a factor influencing their antibacterial properties.[55] The presence of hydroxyl and carboxylate groups on the CQD surfaces provides negative surface charges to effectively interact with Gram-positive bacteria, thus inhibiting their growth. By doping with heteroatoms, the presence of the sulphoxide group on the surface of CQDs further enhances the negative charge, which increases the inhibition efficiency on Gram-positive bacteria, whereas the presence of amine groups on the CQD surface creates a positive surface charge that conversely attracts Gram-negative bacteria, thus causing growth inhibition. Hence, based on previous studies, CQDs are suitable candidates as antibacterial alternatives. Nevertheless, there are limited studies on the antibacterial capabilities of nature-based CQDs, as proven in Table 1.

Although chemical-based CQDs are efficient in inhibiting bacterial growth, the toxic nature of chemicals is still a risk when applied in water quality control, especially in water for consumption. Therefore, the application of nature-based CQDs for antibacterial purposes should be studied to evaluate the efficiency of the CQDs on bacteria inhibition, thus creating a safe and non-toxic antibacterial alternative for water quality control.

In this study, to synthesize chemical-free CQDs for human applications, pure onion juice is selected to synthesize bio-based CQDs. Onion juice is selected due to its nitrogen and sulphur compound contents, which are found to be efficient in enhancing the fluorescent properties of CQDs.[56] The synthesis method, precursors employed, as well as other synthetic parameters, including volume, pH, and temperature, can affect the properties of the CQDs, such as their structure, fluorescence, and solubility. Thus, CQDs with diverse features can be synthesized by altering the aforementioned parameters, making them useful in applications, such as biosensors and bioimaging. Most CQDs can only be excited within the UV region, which limits the practicability in most applications due to the harmful nature of UV light. To enhance their feasibility for antibacterial applications, CQDs need to be doped with functional groups that will red-shift the excitation region to the visible region.

The stability of the CQDs is one of the prerequisites for their practical applications. Previous studies did not perform stability tests on the synthesized CQDs, which calls into question their viability in practical applications, since stability tests need to be conducted to determine their shelf life. Due to the lack of antibacterial studies using nature-based CQDs, as a green alternative to antibiotics, the antibacterial properties of the optimized CQD sample have been analysed by applying them to *E. coli* and *S. aureus* strains, which represent Gram-negative and Gram-positive bacteria, respectively.

Experimental methodology

Yellow onions, lemons, and fine granulated sugar were purchased from a local supermarket in Puchong, Selangor for the synthesis of CQDs. The yellow onions were sliced and blended with the skin. Pure onion juice was then obtained from the blended onions. The lemons were also sliced and blended with the skin to obtain the pure lemon juice. Fine granulated sugar was weighed using an analytical weighing balance (A&D Company Limited, Model HR-250AZ, Japan). After preparing the required mixtures, CQDs were then subjected to either the hydrothermal process or the microwave irradiation process.

Preparation, synthesis, and purification of CQDs

For the initial hydrothermal method test, 50 mL of pure onion juice was prepared and transferred into a Teflon-lined vessel, which was then placed into a polytetrafluoroethylene-equipped stainless-steel autoclave. The autoclave was then subjected to the hydrothermal process at 120 °C for 3 hours using a scientific vacuum oven (MEMMERT GmbH + Co.KG, model VO200, Germany). The process is shown in Fig. 1. Subsequently, the resulting solution was centrifuged at 10 000 rpm for 3 minutes (YingTai, model TG16, China) to separate any large particles. For further purification, the centrifuged solution was filtered through filter paper. A 0.22 μm syringe filter was then used to further remove any unwanted large residues from the product. The mixture was then further dialyzed using a 1 kDa membrane for 12 hours. Fig. 1 shows an illustration of the purification process.

To produce dried CQDs, the purified liquid CQDs were then poured into a covered sample cup and placed in a vacuum oven. The CQDs were heated at 160 °C for 12 hours under vacuum conditions. To prevent any spilling or any loss due to evaporation, the sample cup was covered and sealed shut before heating. Inspired by He *et al.*,[57] the microwave irradiation process was utilized as an alternative green synthesis method to the hydrothermal method. Due to both methods being temperature-assisted reactions, the microwave irradiation method was also reported to have successfully synthesized CQDs. However, there had not been any studies comparing both synthesis methods, which resulted in nature-based CQDs. Hence, as a comparison, for the initial microwave irradiation test, a similar volume of pure onion juice was prepared, then transferred into a beaker and placed into a commercial microwave oven (Samsung, model MS28F303TFK/SM, Malaysia). The sample was heated at 850 W for 3 minutes. Fig. 1 illustrates the procedure for the microwave irradiation method. Similar to the previous purification process, the resulting solution from the microwave irradiation process was centrifuged at 10 000 rpm for 3 minutes. Filter paper and a 0.22 μm syringe were then used to filter and further purify the CQDs, as shown in Fig. 1.

To determine the quantum yields of the CQDs, an optimization study was done, which included manipulating both the surface passivation and synthesis conditions. The surface passivation optimization study was performed to determine the best mixture, as well as the best ratio, to produce CQDs with the best yield. For the surface passivation of the CQDs, pure lemon juice and sugar were mixed with pure onion juice to enhance the quantum yield. For a better comparison, the synthesis conditions were maintained similar to the initial test, including the synthesis temperature, time, and volume. In this part of the

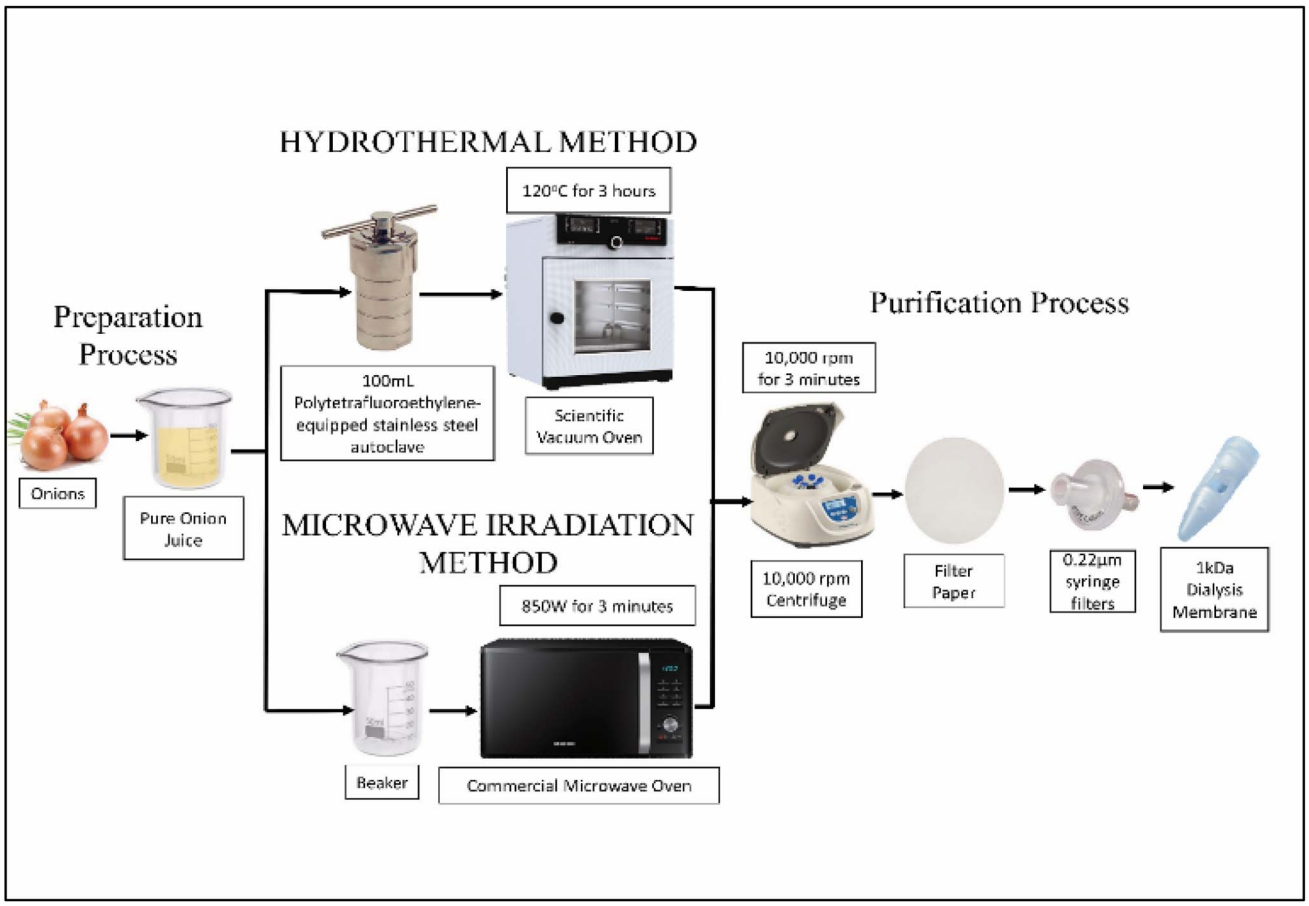

Fig. 1 Preparation, synthesis, and purification of CQDs.

Table 2 Summarized conditions, results, and limitations of CQDs in antibacterial applications

Type of mixture	Ratio
Onion–sugar mixture	Ratio of onion : sugar
	3 : 7
	4 : 6
	5 : 5
	6 : 4
	7 : 3
Onion–lemon mixture	Ratio of onion : lemon
	3 : 7
	4 : 6
	5 : 5
	6 : 4
	7 : 3
Onion–lemon–sugar mixture	Ratio of onion : lemon : sugar
	3 : 7 : 7
	4 : 6 : 6
	5 : 5 : 5
	6 : 4 : 4
	7 : 3 : 3

study, different ratios of three different types of mixtures were prepared in the same volume of 50 mL, as shown in Table 2. All the mixtures were synthesized *via* both the hydrothermal and microwave irradiation methods for further comparison. The ratios were kept the same for all three types of mixtures for a clear comparison of the results.

Characterization of CQDs

Based on previous studies,[29–31,58] CQDs are known to be amorphous nanoparticles smaller than 10 nm that fluoresce when excited. Nitrogen and sulphur-based functional groups are known to be located on the surface of N,S-CQDs.[58] Therefore, to verify that the synthesized product is CQD, an array of characterization processes was done, including physical and chemical property characterization. For physical properties, fluorescence spectroscopy, high-resolution transmission electron microscopy (HRTEM), X-ray diffraction (XRD), and zeta potential measurements were performed to determine the optical properties, size, crystallinity, as well as surface charge of the CQDs. On the other hand, Fourier transform infrared (FTIR) spectroscopy and MTT (3-(4, 5-dimethylthiazolyl-2)-2, 5-diphenyltetrazolium bromide) assay were conducted to characterize the chemical properties of the CQDs, namely the functional groups and cytotoxicity of the CQDs.

Physical property characterization

Fluorescence measurements were carried out using a fluorescence spectrophotometer (Jasco, model FP8300, Japan)

equipped with a quartz cuvette. Here, 3-D measurements were conducted to determine the presence of fluorescence from the sample when it is excited. The 3-D measurement, or more precisely, the 3-D fluorescence spectrum, is an excitation-emission matrix (EEM). Using both excitation and emission monochromators successively, emission spectra for different excitation wavelengths can be measured. Therefore, at different excitation wavelengths, a collection of emission spectra is obtained at the same time. Therefore, the measurement obtained will include two dimensions: emission wavelength and excitation wavelength. The measurement also provides a fluorescence map of all the fluorophores in the mixture, thus enabling their concomitant characterization.[60]

Using a dropper, 3 mL of the sample was inserted into a cuvette, then placed carefully into the integrating sphere of the fluorescence spectrophotometer. The approximate wavelength of both the excitation and emission peaks was determined from the 3-D measurement. This was done by locating the highest fluorescence intensity in the spectrum based on the intensity level chart provided next to the spectrum.

The emission spectrum reflects the probability distribution of the various transitions from the lowest vibrational level, S_1, to the various vibrational levels, S_0. Therefore, it is almost similar to a variation of the luminescence light emission intensity as a function of constant excitation wavelength.[59]

Using the excitation peak obtained from the 3-D measurement, emission spectra were obtained using spectral analysis *via* a fluorescence spectrophotometer. An empty cuvette was placed into the integrating sphere to carry out the analysis before inserting the cuvettes containing 3 mL of sample. This is because air was used as a reference for the analysis. Emission spectra were then plotted from the data recorded. Using the data, the external quantum efficiency or quantum yield percentage was determined using eqn (1).[60]

$$\text{External quantum efficiency}(\%) = \frac{\text{absorptance}(\%)}{100\%} \times \text{internal quantum efficiency}(\%) \quad (1)$$

Meanwhile, HRTEM images were obtained using a high-resolution transmission electron microscope (JEOL, model JEM-2100F, Japan, accelerating voltage of 200 kV) to determine the size and morphology of the CQD sample. The CQD samples in the liquid phase were drop-cast onto a Formvar copper grid, and the grid was air-dried at room temperature for HRTEM analysis. HRTEM (a mode of Transmission Electron Microscopy (TEM) imaging) enables the visualization of the crystallographic arrangement of a specimen at the atomic scale. In contrast to traditional microscopy techniques, this approach does not rely on absorption mechanisms to generate images; instead, image formation is based on interference effects in the image plane. Electrons interact with the specimen independently, traversing the imaging system where phase shifts occur and interference takes place. The resulting image does not directly depict the structural features of the specimen. This technique serves as a crucial instrument for investigating the nanoscale characteristics of materials owing to its exceptional spatial resolution.[61] The capability of imaging crystal structures,[62] crystal defects, and even individual atoms[63] is achievable due to this remarkable level of resolution.

XRD studies were conducted using an X-ray diffractometer (Malvern Panalytical, model EMPYREAN, United Kingdom) at a scanning rate of 5° min^{-1}. between 10° and 60° (2θ). XRD analysis was done to determine the crystallinity of the sample. XRD serves as a crucial method in the study of both amorphous and semi-crystalline polymers.[64,65] It enables the comprehensive analysis of various features of the material's microstructure, such as lattice parameters, presence of defects, crystallographic orientations (texture), and level of crystallinity.

During a typical X-ray diffraction experiment, the sample undergoes exposure to X-ray radiation, a type of short-wavelength ($\lambda \approx 0.1$ nm) electromagnetic radiation. Typically, the X-ray radiation is generated by bombarding a metal target with high-speed electrons within a vacuum tube. This generation process often results in two components of radiation: a continuous spectrum of white radiation and a superimposed line spectrum with a frequency contingent on the bombarded metal. As the X-ray beam traverses the sample, its intensity diminishes exponentially: $I = I_0 \exp(-\mu x)$, where I_0 represents the initial intensity and μ signifies a linear absorption constant. Consequently, the depth of X-ray penetration is influenced by both the material properties and the X-ray source's energy.[66]

The incident X-ray beam experiences partial absorption, partial scattering, and the remaining portion transmits through the specimen without alteration. Scattering arises from the interaction between the incident X-rays and the material's electrons, while the diffracted X-rays further interact to produce diffraction patterns that are dependent on the incident beam's angle relative to the specimen's orientation. Notably, the terms scattering and diffraction are often used interchangeably in this context. X-ray diffraction also proves valuable in the examination of amorphous polymers. The diffraction patterns observed in amorphous polymers lack the distinct peaks characteristic of crystals, instead displaying broader features. A quantitative analysis of diffraction patterns from amorphous polymers can yield critical insights into the local atomic structure, encompassing details such as bond lengths, morphology, and radial distribution information.[66]

For zeta potential measurement, the CQD samples were loaded into folded capillary zeta cells (DTS1070, Malvern Instruments, Worcestershire, UK). The surface charge characteristics of the samples were analyzed at 25 °C with a Zetasizer Nano ZS (Malvern Instruments, Worcestershire, UK) equipped with a 633 nm laser.

Chemical properties characterization

FTIR spectroscopy was conducted using an FTIR spectrophotometer (PerkinElmer, Model Frontier, Massachusetts, USA) in ATR mode on scanning frequencies ranging from 4000 cm^{-1} to 650 cm^{-1}, to determine the surface functional groups of the CQD sample. Infrared (IR) spectroscopy involves the measurement of infrared light interacting with a molecule. It is normally

used to determine the functional groups in molecules by measuring the vibrations of atoms within the molecules. Light atoms and stronger bonds tend to vibrate at a high stretching wavenumber or frequency.[67] Fourier-transform infrared (FTIR) analysis measures the wavelength range in the IR region absorbed by a material by applying IR radiation to a sample of the material. The absorbance of the sample is then used to determine the molecular structure and composition of the material.[68]

Before obtaining IR Spectra, a background scan was performed to remove any surrounding noises that, if not removed, would cover up some functional groups during analysis. After the background scan was done, one drop of the sample was placed onto the diamond cell on the Attenuated Total Reflectance (ATR) plate using a dropper. After the clamp was screwed down, IR spectral analysis was performed. It was suggested that after every analysis, ethanol and Kimwipes could be used to carefully clean the sensor. IR spectra were then plotted from the data recorded. To determine the functional groups in the samples, the IR spectrum table was referred to; it lists the IR spectroscopy frequency ranges, the appearance of the vibrations, and the absorptions of functional groups. The frequency was found in the first column of the table, then the corresponding absorption, appearance, group, and compound class were determined.[69]

For cytotoxicity, the MTT assay was performed on HeLa cells. The HeLa cells (5×10^4 cells per well) were seeded into 96-well plates and incubated in a humidified CO_2 incubator at 37 °C, and supplemented with 5% CO_2. The spent medium was aspirated from each well and washed with 100 μL of phosphate-buffered saline (pH 7.4). CQDs of varying concentrations were transferred to each well and allowed to incubate for 24 hours in a humidified CO_2 incubator at 37 °C, supplemented with 5% CO_2. The spent medium was aspirated from each well and washed with 100 μL of phosphate-buffered saline (pH 7.4). Next, 100 μL of fresh media was added to each well, followed by 20 μL of 5 mg mL^{-1} MTT solution. The plate was shaken gently and further incubated for 4 hours at 37 °C. After incubation, the spent medium was fully aspirated, and the purple formazan crystals were solubilized with 100 μL of DMSO. The plates were incubated at room temperature with gentle shaking for 10 minutes, and the absorbance was taken with an ELISA plate reader at 570 nm wavelength.

Stability of CQDs

Due to the lack of stability determination in previous studies, a stability test was conducted *via* fluorescence measurements to determine the "shelf-life" of the CQDs synthesized. The fluorescence measurements were carried out in a fluorescence spectrophotometer (Jasco, model FP8300, Japan) equipped with a quartz cuvette. After every measurement, the sample was stored in a fridge until the next measurement. The 3-D fluorescence spectra and external quantum efficiency were measured daily for a period of 180 days.

Antibacterial activity of CQDs

Wild-type strains of *E. coli* (ATCC25922) and *S. aureus* (ATCC25923) were utilized throughout the experiment, including the minimal inhibitory concentration (MIC) test and zeta potential analysis. The bacteria were grown in Mueller-Hinton broth media at 37 °C.

The minimum inhibitory concentration (MIC) is a standardized method used to determine the precise concentration of an antimicrobial agent required to inhibit microbial growth.[70] The authors consider this technique particularly relevant to the current study, as it enables the identification of the lowest concentration of optimized carbon quantum dots (CQDs) that effectively suppresses visible bacterial growth. For the MIC test, *S. aureus* (ATCC 25923) and *E. coli* (ATCC 25922) were cultured overnight in tryptic soy broth (TSB) at 37 °C with agitation at 180 rpm. Bacterial concentrations were adjusted to an optical density (OD595) of 0.11 to obtain 1.5×10^8 CFU mL^{-1} of bacterial suspension. In a 96-well cell culture plate, 50 μL of bacterial cell suspension was added to each well, followed by the addition of 50 μL of various concentrations of CQD, resulting in a final volume of 100 μL per well. As a positive control, 50 μL of tetracycline (250 μg mL^{-1}) was added to a well containing bacterial cell suspension, while a well with bacterial suspension in TSB without CQD served as the control. The plate was then incubated at 37 °C with agitation at 180 rpm for 48 hours. Bacterial concentrations were measured at 595 nm at two-hour intervals for the first 24 hours and every four hours between 24–48 hours. This experiment was performed in triplicate.

Evaluation of the antibacterial mechanism

To evaluate the antibacterial mechanism of the CQDs, the zeta potentials of the bacteria before and after treatment with CQDs were analysed. The zeta potential or electrokinetic potential[71] was ascertained through the collective electrical charge of molecules exposed on the surface, representing an indirect approach for evaluating the surface potential of bacteria. This fundamental attribute is crucial for upholding the optimal functionality of cells. Additionally, it exerts a significant influence on the attachment of bacteria to substrates and their interaction with various environmental factors.

Hence, to test the antibacterial effect of charged CQDs towards bacteria, zeta potential analysis was performed to measure the surface charge of the bacteria before and after the interaction between the bacteria and CQDs. Based on the MIC test, the CQD samples were prepared at optimal concentrations in water. Both *S. aureus* (ATCC 25923) and *E. coli* (ATCC 25922) were cultured overnight in tryptic soy broth (TSB) at 37 °C with agitation at 180 rpm. Bacterial concentrations were adjusted to an optical density (OD595) of 0.11 to obtain 1.5×10^8 CFU mL^{-1} of bacterial suspension and incubated with the CQD samples (1 : 1 v/v) in a 96-well microtiter plate for 36 hours. The samples were loaded into folded capillary zeta cells (DTS1070, Malvern Instruments, Worcestershire, UK). The surface charge characteristics of the samples were determined at 25 °C with a Zetasizer Nano ZS (Malvern Instruments, Worcestershire, UK) equipped with a 633 nm laser.

To further verify the antibacterial effect of the CQDs against the bacteria, SEM was performed to observe the morphology or

shape of the bacteria before and after treatment with CQDs. The utilization of scanning electron microscopy (SEM) represents a robust methodology specifically crafted for the analysis of the surface characteristics of various materials.[72] Within the SEM framework, a high-energy electron beam is meticulously directed towards the material specimen, often reaching acceleration voltages of around 30 kV, as outlined by Inkson.[73] This process instigates a series of interactions between the electron beam and the specimen, resulting in the emission of signals from the material, subsequently captured by specialized detectors.

To perform SEM, a bacterial culture was prepared by inoculating 10 mL of TSB with a single *E. coli* colony and incubating at 37 °C with shaking until OD600 = 0.6. The bacterial culture was then pelleted at 4000×*g* for 5 min and resuspended with 500 mg mL^{-1} CQD diluted in TSB for 2 hours. The procedures were repeated by replacing *E. coli* with *S. aureus*. After treatment, the bacteria were centrifuged and washed twice with 5 mL of PBS solution. The samples were then fixed in 4% glutaraldehyde solution for 6 hours at 4 °C, then centrifuged and washed with 0.1 M sodium cacodylate buffer (three times, 10 minutes each). The bacterial pellet was then subjected to postfixation treatment by incubation in 1% osmium tetroxide for 2 hours at 4 °C and subsequent washing with 0.1 M sodium cacodylate buffer (three times, 10 min each). Subsequently, the fixed samples were dehydrated by washing with a series of acetone solutions and the resulting samples were transferred to an aluminum foil (1 cm^2) precoated with albumin solution and subjected to critical point drying for 1.5 hours. The samples were mounted on a metal stub and coated with gold in a sputter coater (Bal-Tec, model SCD005, Liechtenstein). The samples were observed under the scanning electron microscope (JEOL Ltd, model JSM-IT100, Japan).

To further prove that the CQDs possess antibacterial properties, an isotype test was carried out with two other bacterial strains, namely *S. ser. Typhimurium* (ATCC 13311) and *V. parahaemolyticus* (ATCC 17802). In this test, the Kirby–Bauer disk diffusion method was used to quickly determine the antibacterial properties of the CQDs against the above-mentioned bacterial strains. A single isolated colony of *S. ser. Typhimurium* was chosen and inoculated into 5 mL of TSB medium and grown overnight at 37 °C with shaking at 180 rpm. Subsequently, 50 μL of each diluted sample was applied to a filter paper disk and allowed to dry in a laminar air stream. Subsequently, 150 μL of the bacterial culture was spread evenly onto tryptic soy agar (TSA) using a sterile cotton swab, while excess liquid on the agar was allowed to dry under a laminar hood. Filter paper discs in which test samples were embedded were then placed on the TSA with sufficient space between the discs. The procedures were repeated using *S. ser. Typhimurium* replaced with *V. parahaemolyticus*. The plates were finally incubated at 37 °C for 8 hours, and the resulting zone of inhibition was measured.

Results

Excitation and emission peak determination

CQDs synthesized *via* the hydrothermal method were subjected to 3-D measurements to obtain both excitation and emission peaks.

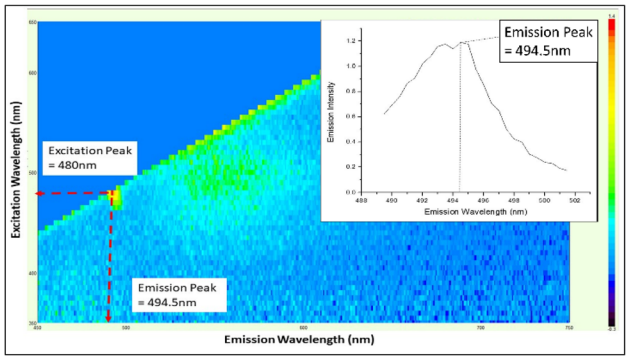

Fig. 2 3-D measurement of the excitation wavelength and emission wavelength for CQDs produced *via* the hydrothermal method. Inset shows the corresponding emission spectrum.

Excitation and emission peaks are the points in the wavelength where the maximum fluorescence intensity is detected from the sample. This means that when the sample is excited at the excitation peak wavelength, the highest fluorescence intensity can be detected at the emission peak wavelength. This is important for determining the optimum wavelength to excite the sample and its emission wavelength.

Fig. 2 shows that CQDs synthesized *via* the hydrothermal method exhibit an excitation peak of 480 nm and an emission peak of 494.5 nm, which indicates that the emission peak is in the blue region; therefore, CQDs synthesized under the hydrothermal method emit blue light when excited.

Based on the emission spectrum attached in Fig. 2, when the CQD sample is excited at 480 nm, emission peak is found at 494.5 nm, thus proving the findings of the 3-D measurement. Hence, at the excitation wavelength of 480 nm, the sample has the strongest absorption. Using the excitation peak obtained from 3-D measurement, the emission spectrum can then be plotted as shown in the inset figure of Fig. 2.

The microwave irradiation method was selected to produce results for comparison with those obtained from the hydrothermal method since it is also a green synthesis method. Moreover, at the industrial scale, microwave irradiation is more cost-effective compared to the hydrothermal method due to its high-volume production.

After the CQDs were synthesized *via* the microwave irradiation method, they were sent for 3-D measurements. In Fig. 3, it is shown that CQDs synthesized *via* the microwave irradiation method exhibit an excitation peak of 480 nm and an emission peak of 493 nm, which indicates that the emission peak is also found in the blue region. Therefore, the CQDs synthesized *via* the hydrothermal method emit blue light when excited. Furthermore, Fig. 3 shows that when 480 nm light hits the sample, the sample will become excited and emit light with an emission peak at 493 nm. Using the excitation peak obtained from the 3-D measurement, the emission spectrum can then be obtained for quantum yield calculation.

Based on the emission spectrum attached in Fig. 3, when the CQD sample is excited at 480 nm, an emission peak is found at 493 nm, thus proving the findings of the 3-D measurement.

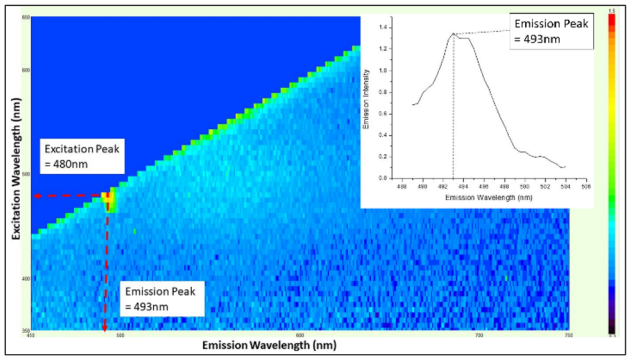

Fig. 3 3-D measurement of the excitation wavelength and the emission wavelength for CQDs produced *via* the microwave irradiation method. Inset shows the corresponding emission spectrum.

Hence, at the excitation peak wavelength of 480 nm, the sample has the strongest absorption. The emission spectrum was then plotted by using the excitation peak obtained from the 3-D measurement, as shown in the inset figure of Fig. 3.

Based on the 3D measurements in Fig. 2 and 3, it was found that the excitation peaks for both methods are similar at 480 nm. However, the emission peak for the hydrothermal CQDs was found at 494.5 nm, while for the microwave irradiation CQDs, the emission peak was at 493 nm. This indicates that CQDs obtained *via* microwave irradiation exhibited a smaller Stokes shift. The Stokes shift is commonly defined as the wavelength difference between the peaks of the excitation and emission spectra.[74] The overlap between both spectra is defined as the reabsorption region or reabsorption loss, where emitted photons from the sample are reabsorbed to excite the remaining unexcited particles.[75] The smaller the Stokes shift, the larger the reabsorption region, thus the lower the amount of emitted photons detected, and the lower the external quantum efficiency, which is also known as quantum yield percentage. The Stokes shift was calculated using eqn (2).

$$\text{Stokes shift} = \text{emission peak} - \text{excitation peak} \quad (2)$$

In this case, since the CQDs obtained by microwave irradiation exhibited a smaller Stokes shift in comparison to hydrothermal CQDs, the microwave irradiation method may result in a lower quantum yield percentage.

Quantum yield determination

To calculate the quantum yield of the CQD sample, distilled water was used as a reference. Using the Spectra Manager spectroscopy software, the external quantum efficiency of the CQD sample from the hydrothermal method was found to be 0.218%. This states that for every 10^5 photons absorbed by the sample, only 218 photons are emitted by the sample. Therefore, by determining the quantum yield, it can be determined that the efficiency of this CQD sample is 0.223%.

For the CQD sample that had undergone microwave irradiation, the external quantum efficiency was found to be 0.144%. This states that for every 10^5 photons absorbed by the sample, only 144 photons are emitted by the sample. Therefore, by determining the quantum yield, it can be determined that the efficiency of this CQD sample is 0.144%.

As explained in the previous section, the smaller the Stokes shift, the lower the external quantum efficiency. The microwave irradiation CQDs exhibited a smaller Stokes shift in comparison to the hydrothermal CQDs, resulting in a lower quantum yield percentage. The smaller Stokes shift may be due to the different synthesis methods. It was discovered in previous studies that onion CQDs exhibited a higher quantum yield percentage for the hydrothermal method,[37] which was proven in the results in the first section.

However, the optimum synthesis method may be different when some parameters, such as volume and type of mixtures, are altered. To test this, and also to determine the optimized conditions for synthesizing CQDs of the highest quantum yield, CQDs were synthesized according to a series of parameters and then tested for their quantum yield percentages. The parameters include the type of enhancement materials and the ratio of mixture, volume, and pH.

Surface passivation of CQDs

For this part, lemon juice and sugar were selected as enhancement materials to increase the quantum yield percentage of the CQDs. Based on Table 2, CQDs were synthesized and subjected to 3-D measurements as well as quantum yield calculations. Fig. 4 shows the highest quantum yield percentage results based on the mixtures and synthesis methods. According to the results shown in Fig. 4, it was found that for both synthesis methods, the addition of sugar and lemon increased the quantum yield of the CQDs. This proves that surface passivation was successful in enhancing the yield of CQDs, especially for the microwave irradiation method, which showed a significant increase in comparison to the yield of CQDs produced from pure onion juice. Moreover, an onion–sugar mixture with a ratio of 3 : 7 has surpassed the other mixtures in terms of quantum yield percentage in both synthesis methods. This proves that in comparison to pure lemon juice, sugar would be a better material for the surface passivation of onion-based CQDs. In terms of the type of mixtures, although lemon juice is a good source of citric acid, its low pH drastically reduced the fluorescence of the CQDs produced. The optimum pH for highest

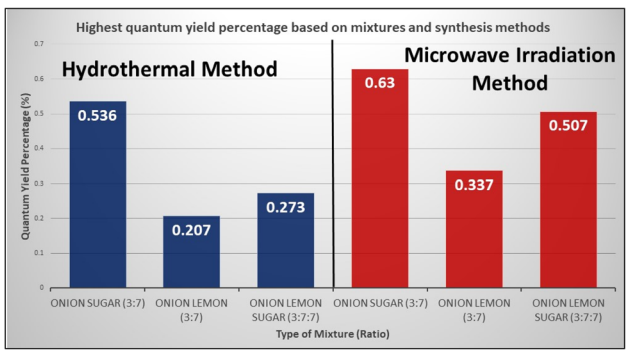

Fig. 4 Highest quantum yield percentages of CQDs based on mixtures and synthesis methods.

fluorescence was previously reported to be at pH 7.0; any increase or decrease in pH would reduce the fluorescence.[76] Therefore, in this case, the onion–sugar mixture produced the highest quantum yield in comparison to both the onion–lemon and onion–lemon–sugar mixtures. In terms of ratio, it was found that when the onion ratio increased, the quantum yield percentage decreased. This may be due to the decrease in sugar, which is the main carbohydrate source of the CQDs. However, when the onion ratio was further decreased, the quantum yield percentage also decreased, which contradicts the previous statement. This is due to the S-doping of the CQDs by the sulphur-containing onion juice. A previous study by Lu *et al.*[33] had proven that the introduction of S-dopants into CQDs would cause a red-shift of the maximum emission wavelength. The corresponding red-shift would cause an increase in the Stokes shift, thus reducing the reabsorption loss and increasing the quantum yield percentage of the CQDs. Therefore, in this case, the reduction in onion juice resulted in the decrease in S-dopants, and thus the quantum yield percentage was inadvertently reduced. As a result, an optimum onion–sugar ratio of 3 : 7 was discovered to synthesize CQDs of the highest quantum yield percentage compared with the other ratios.

Nevertheless, it was found that in terms of synthesis method, due to the addition of the enhancement materials, microwave-irradiation-treated CQDs exhibited a higher quantum yield percentage (0.630%) than the hydrothermal-treated CQDs (0.536%). In amorphous carbon quantum dots (CQDs), the lack of long-range structural order means that surface defects and functional groups such as –OH, –COOH, and $–NH_3$ play a dominant role in photoluminescence. As a result, the emission behavior tends to be highly excitation-dependent, which correlates with a very low quantum yield.[77] Based on the results, the optimized mixture was determined to be an onion–sugar ratio of 3 : 7 under the microwave irradiation method. To further study the quantum yield extent of the surface-passivated CQDs, the synthesis conditions were manipulated to determine the optimized conditions for CQD synthesis.

Synthesis condition optimization

To start, we investigated the effects of volume on quantum yield percentage. Based on previous results, the mixture with the highest quantum yield percentage was used, which is the onion–sugar mixture ratio of 3 : 7 under the microwave irradiation method. In this part, the CQDs were synthesized as reported previously. However, instead of 50 mL, the volume was increased to 100 mL, 150 mL, 200 mL, and 250 mL. Fig. 5 shows the quantum yield percentage of the CQDs based on the volume of the mixture.

Based on the results in Fig. 5, the higher the volume of the onion–sugar mixture, the higher the quantum yield percentage of the synthesized CQDs. At 250 mL, the CQDs achieved 1.4 times the quantum yield percentage in comparison to the initial 50 mL mixture.

This is perhaps due to the increase in fluorophore concentration. When the volume is increased, more CQDs will be synthesized from the larger mixture volume, thus resulting in a higher fluorophore concentration. The increase in the

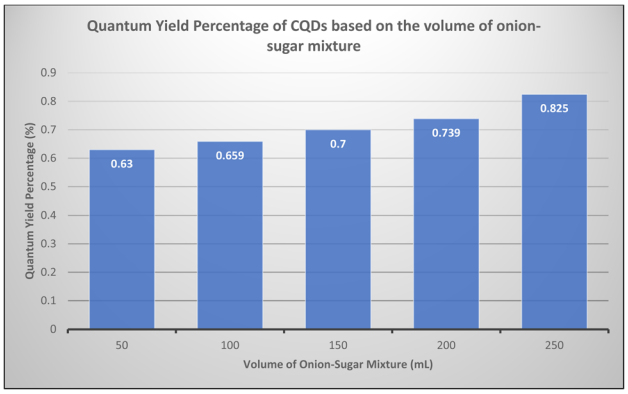

Fig. 5 Quantum yield percentages of CQDs based on the volume of the onion–sugar mixture.

fluorophore concentration results in a higher number of molecules within the detection volume and eventually leads to a higher quantum yield percentage. This also proves that the CQDs are suitable for industrial-scale production and not necessarily just for lab experiments.

The effect of pH on the quantum yield percentage of the CQDs was also studied. Before the pH manipulation, the pH of the produced CQD solution was 4.6. The effects of the pH manipulation on the quantum yield percentage are shown in Fig. 6. Here, the quantum yield percentage increases as the pH increases until it reaches pH 7.6, beyond which it decreases even as the pH increases. This means that at pH 7–8, the CQDs exhibit the highest quantum yield percentage. Thus, the optimal pH would be between pH 7 and 8.

This result corresponds with the previous statement on the optimum pH discovered, which is pH 7.[76] This shows that the CQDs synthesized in this study work less efficiently in both acidic and alkaline conditions, which is a desirable outcome for consumer applications. If the CQDs work effectively in either acidic or alkaline conditions, then chemicals would be required to maintain the pH condition of the CQDs, which in turn may be harmful to consumers if not carefully implemented.

Verification of optimized CQD sample

Based on the current available results, the optimal conditions are as follows: CQDs at pH 7–8, produced from a 250 mL onion–

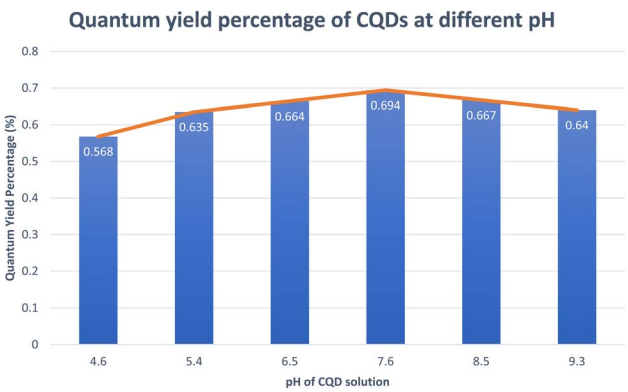

Fig. 6 Quantum yield percentage of CQDs at different pH values.

sugar mixture, with a ratio of 3 : 7 *via* the microwave irradiation method. Based on the CHNS analysis, the synthesized CQDs consist of 43.2% carbon, 6.6% hydrogen, and 0.6% nitrogen. The 3-D spectrum, as well as the emission spectrum of the optimum CQDs, is shown in Fig. 7, and the quantum yield percentage is 2.101%.

Based on the results, in terms of quantum yield calculation, the optimized CQDs are 9.4 times higher than the yield of the synthesized CQDs of the initial hydrothermal method, and 14.6 times higher than the yield of the initial microwave irradiation method. This proves that the optimization was a complete success. Furthermore, based on the results in the 3-D spectrum, the excitation peak was found at 470 nm, while the emission peak was at 541 nm. This proves that visible light can be used to excite the CQDs. Fig. 8 shows the photo of the CQDs under normal light and UV light.

After synthesizing CQDs under the optimal conditions, the quantum yield percentage was significantly higher than the yield from the initial onion CQDs. This proves that the enhancements and optimum conditions imposed on the initial onion CQDs were successful in improving the yield. Furthermore, as shown in Fig. 7, the optimum CQDs had a larger Stokes shift, which is one of the reasons that led to the increase in quantum yield percentage. Other than the red-shift of the emission peak, a blue-shift in the excitation peak was also observed; this was due to the enhancements and optimal conditions. The fluorescence of the CQDs is reportedly prone to manipulation *via* the tuning of a variety of parameters, such as size, pH, and type of materials.[78] In this study, by tuning the type of materials, pH, and volume, the fluorescence of the CQDs displayed significantly different results, thus proving the theory. The CQD sample was also subjected to UV light exposure under dark conditions to verify the fluorescence of the sample. Despite the excitation maxima in the visible light region and not the UV region, the fluorescence could not be seen clearly under visible light, as fluorescence makes little difference to the light used to excite the nanoparticles. Thus, by using UV light, the nanoparticles would have emitted visible light fluorescence, which could cause a big difference to be seen by the naked eye. As shown in Fig. 8, under UV light, the colour of the CQDs changed from brown-orange to green, thus proving that the CQDs exhibit fluorescence when excited.

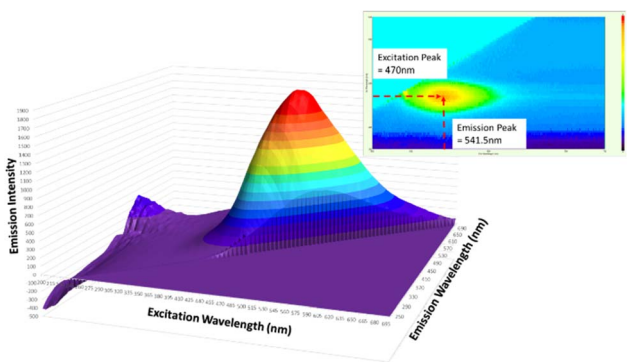

Fig. 7 3-D Plot of the fluorescence spectra of the optimized CQDs.

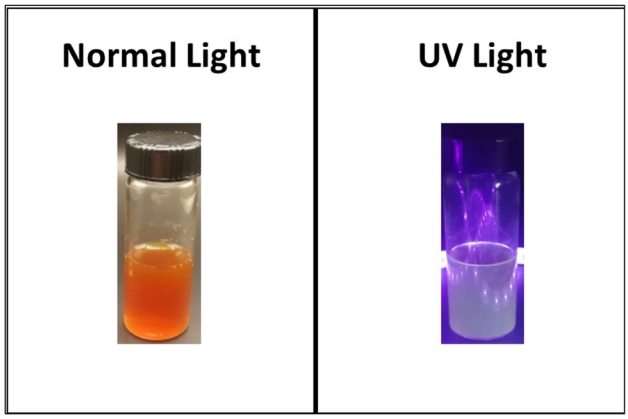

Fig. 8 CQDs under normal light (left) and under UV light (right).

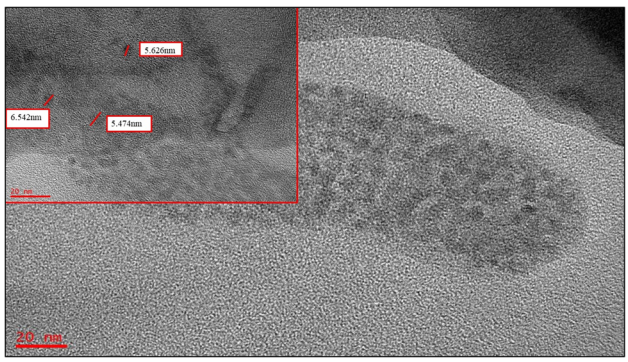

Fig. 9 HRTEM image of the optimized CQDs on a layer of Formvar sheet within a copper grid at a magnification of 120 000; the inset shows a magnification of 200 000.

Particle size and morphology determination

After the optimized CQDs were produced, they were subjected to HRTEM to determine the size and morphology of the CQDs. Fig. 9 shows the HRTEM images of the optimized CQDs at magnifications of 120 000 and 200 000. Fig. 10 shows the particle size distribution chart of the optimized CQDs. Fig. 9 and 10 are proof of the presence of uniform, spherical particles with average sizes ranging from 4–6 nm.

As shown in Fig. 9, the nanoparticles are spherical, and the average particle size was between 4 and 6 nm, as shown in the histogram in Fig. 10. This has further proven that the nanoparticles synthesized are considered CQDs due to the nanoparticles being spherical and the particle size being smaller than 10 nm, as defined by Oliveira and Alves.[79] The HR-TEM image demonstrates aggregate layers due to the amorphous nature of the synthesized CQDs, as confirmed by XRD analysis; they lack the short-range structural order necessary to produce visible lattice fringes.

Amorphous structure determination

To determine the crystallinity of the CQD sample, the optimized CQDs were sent for XRD analysis. Fig. 11 shows the XRD crystallinity graph of the optimized CQDs. The XRD pattern of the

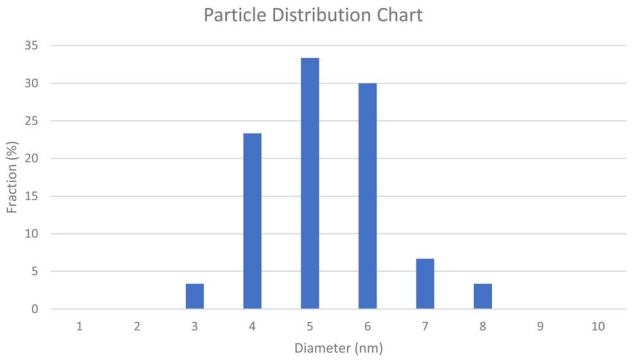

Fig. 10 Particle size distribution chart for the optimized CQDs.

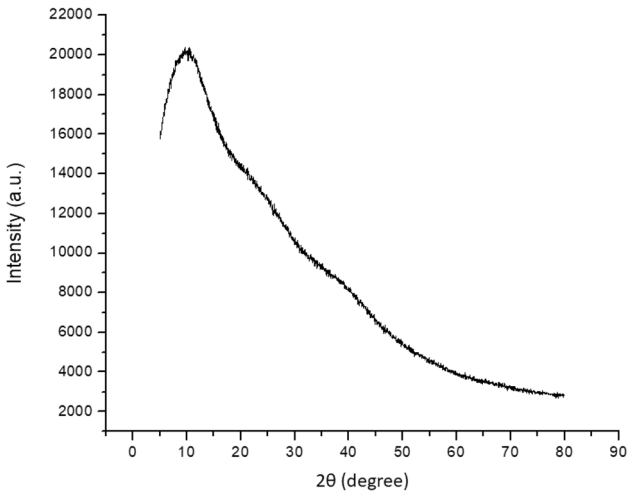

Fig. 11 XRD crystallinity graph of the optimized CQDs.

CQDs showed a broad peak at approximately $2\theta = 9.5°$, and the interlayer spacing (d) of the CQDs (0.93 nm) was higher than the graphitic interlayer spacing (0.33 nm); this is proof that the CQDs synthesized are amorphous.

Unlike crystalline-structured CQDs, amorphous variants are known to be water-soluble and bio-compatible.[80] These characteristics are beneficial for *in vivo* applications, such as nano-antibiotics and bioimaging. Previous studies concluded that properties exhibited by amorphous variants are similar to those of the crystalline variants. Cao *et al.*[81] had proven that the spectroscopic properties of the photoluminescence emissions exhibited by both amorphous and crystalline variants are almost similar, including the well-known excitation-dependent emission property. Hence, the amorphous CQDs synthesized in this study would be suitable for antibacterial applications.

Cytotoxicity determination

To determine the cytotoxicity, the CQDs were subjected to an MTT assay on HeLa cells. Fig. 12 shows the results obtained from the MTT assay. Differing from previous studies, the MTT assay conducted in this research studied the cytotoxicity of CQDs at the mg mL^{-1} concentration instead of the μg mL^{-1} concentration. Based on Fig. 13, the cell viability of HeLa cells

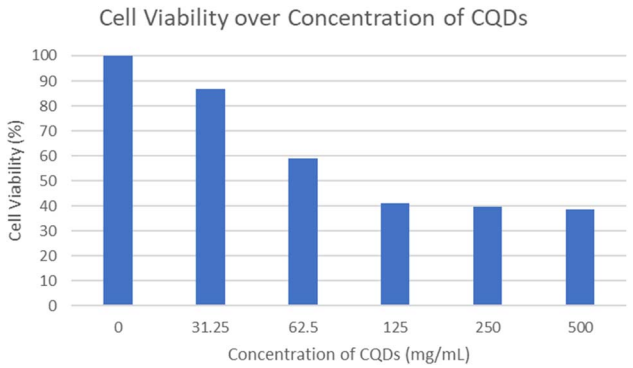

Fig. 12 HeLa cell viability at various concentrations of CQDs.

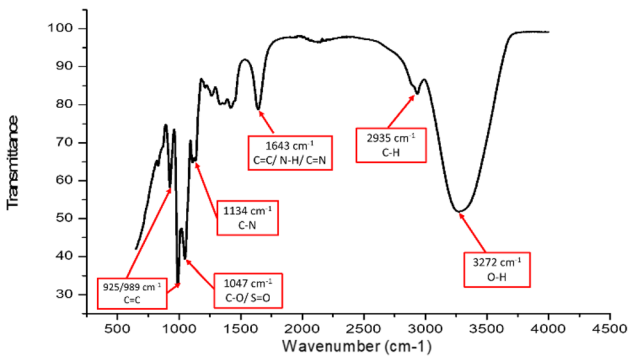

Fig. 13 FTIR spectrum of the optimized CQDs.

was found to be lower than 50% before reaching 125 mg mL^{-1}. This shows that at around 100 mg mL^{-1}, the CQDs were starting to become toxic towards the HeLa cells tested. However, compared to previous studies, the CQDs produced in this study are less cytotoxic since the CQDs tested in previous studies were at μg mL^{-1} concentrations. This might be due to the use of natural-based precursors in this study to synthesize CQDs instead of using chemical-based precursors like previous studies. Table 3 shows the summary of parameters and results of the cytotoxicity tests conducted by previous studies on QDs and CQDs.

Surface functional group determination

To determine the surface functional groups, the optimized CQDs were analyzed using an FTIR spectrometer. By identifying the functional groups, properties of the optimized CQDs, such as water solubility and polarity, were determined.

FTIR analysis can also identify the chemical substances contained in the sample, thus confirming the toxicity of the CQDs. The FTIR analysis results are shown in Fig. 13. The peak at 3272 cm^{-1} is attributed to the stretching vibration of the normal polymeric hydroxyl (O–H); at 2935 cm^{-1}, the medium peak is attributed to the stretching vibration of alkane (C–H); the medium peak at 1643 cm^{-1} can be attributed to the stretching vibrations of conjugated alkene (C=C) and imine (C=N), as well as the bending vibration of amine (N–H); at 1134 cm^{-1}, the medium peak is attributed to the stretching

Table 3 Summary of parameters and results of the cytotoxicity tests from previous studies

Type of nanoparticles	Core/shell	Solvents	Cytotoxicity		References
			Tested cell	Concentration of IC50	
Cd-based quantum dots	CdTe	Tellurium, *N*-acetyl cysteine, $CdCl_2$, and sodium borohydride	*S. cerevisiae*	89.8 nM	83
	CdTe	Tellurium, mercaptoacetic acid, $CdCl_2$, and sodium borohydride	*S. cerevisiae*	56.2 nM	83
	CdTe	Tellurium, glutathione, $CdCl_2$, and sodium borohydride	*S. cerevisiae*	15.3 nM	83
Metal-based quantum dots	ZnO	Zinc acetate dehydrate, hexamethylenetetramine	*KB44* (*C*)	42 μg mL^{-1}	84
			HeLa (*C*)	45 μg mL^{-1}	84
			HFF-2 (*N*)	125 μg mL^{-1}	84
Metal-free quantum dots	CQDs	Onion waste, and EDA	*HEK-293*	1 mg mL^{-1} (IC90)	21
			HeLa	1 mg mL^{-1} (IC90)	21
	NIR-CQDs	Pulp-free lemon juice and formamide	*HeLa*	1 mg mL^{-1} (IC90)	82
	N–S-CQDs	Onion and sugar	*HeLa*	58.26 mg mL^{-1}	Current study

vibration of amine (C–N); the strong peak at 1047 cm^{-1} is attributed to the stretching vibrations of vinyl ether (C–O) and sulfoxide (S=O); the strong and medium peaks at 989 cm^{-1} and 925 cm^{-1} are respectively attributed to the bending vibrations of alkene (C=C). The FTIR spectra show a successful unification of amino groups (1643 cm^{-1}), hydroxyl (3272 cm^{-1}), alkene (989 cm^{-1}), vinyl ether (1047 cm^{-1}), and sulfoxide (1047 cm^{-1}), as well as minor alkane (2935 cm^{-1}) on the CQD surface. Using these findings, the CQD properties could be determined based on the peak strengths. According to the results shown in Fig. 13, the strong peak of the hydroxyl group proves that the CQDs have high solubility and polarity. This means that the CQDs can easily bond with other polar molecules, such as water. This also proves the water-soluble property exhibited by amorphous CQDs mentioned previously. Furthermore, the strong peak of the sulfoxide group indicates the presence of S-dopants on the CQD surface, thus proving that the red-shift of the emission peak was due to the S-doping of the CQDs. Minor peaks of amine and imine were also observed in the FTIR spectrum. This is due to the nitrogen content of the onions, which resulted in the N-doping of the CQDs; therefore, the CQDs were found to be N–S doped.

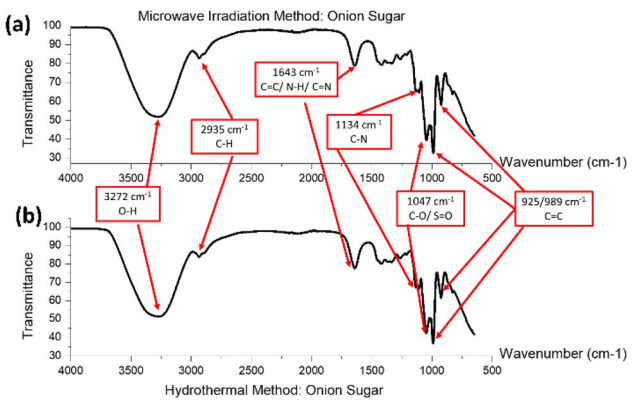

Fig. 14 FTIR spectra of CQDs synthesized using the onion–sugar mixture *via* the (a) microwave irradiation method, and (b) hydrothermal method.

As a comparison, the optimized CQDs synthesized *via* the hydrothermal method instead of the microwave irradiation method were also sent for FTIR analysis. Fig. 14 shows the FTIR results for the microwave irradiation method (a) and the hydrothermal method (b). The CQDs synthesized *via* both methods showed similar peak patterns, thus proving that both methods successfully synthesized N,S-CQDs. However, the microwave irradiation method is more industry-beneficial compared to the hydrothermal method due to its faster synthesis time, hence lower synthesis cost, especially at a larger scale.

Next, optimized CQDs synthesized *via* the microwave irradiation method using the onion–lemon mixture instead of the onion–sugar mixture were also analysed to compare the passivation effects of sugar and lemon on the onion CQDs. Based on Fig. 15, the onion–lemon CQDs overall showed weaker and fewer peaks compared to the onion–sugar CQDs. The weaker O–H peak at 3367 cm^{-1} indicates that the onion–lemon CQDs have lower solubility and polarity compared to the onion–sugar CQDs. Moreover, the absence of peaks for the onion–lemon CQDs might be due to the lack of carbohydrates during the carbonization process, thus having less variety of surface passivation in comparison to onion–sugar CQDs. Furthermore, due to the lack of sulphur compounds on the CQD surface, onion–lemon CQDs seem to be N-doped instead of N,S-doped, which massively reduced the performance of the CQDs, as proved by the quantum yield percentage results in Fig. 5, thus suggesting once again that effective surface passivation is crucial in producing CQDs with high quantum yield percentage.

Surface charge determination

The surface functional groups are expected to affect the surface charge of the CQDs. The CQDs were found to exhibit a charge of −5.83 mV, which shows that the CQDs are negatively charged.

Stability of CQDs. To determine the stability of the CQDs, fluorescence measurements were performed on the optimized

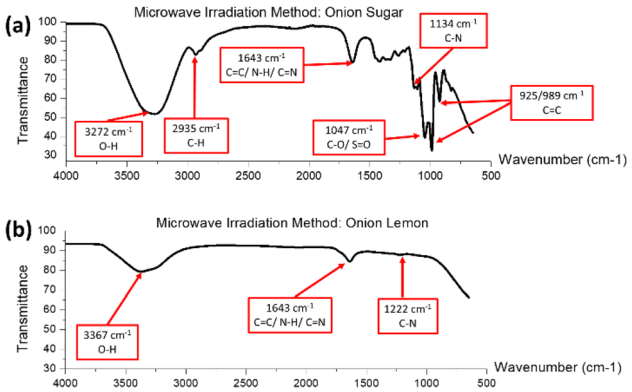

Fig. 15 FTIR spectra of CQDs synthesized using the onion–sugar mixture *via* the (a) microwave irradiation method and (b) hydrothermal method.

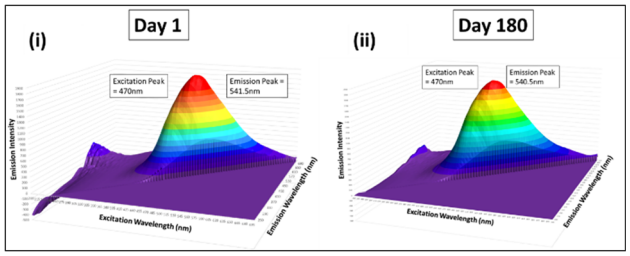

Fig. 16 3-D plot for fluorescence spectra of the optimized CQDs on (i) day 1 and (ii) day 180.

CQD sample daily for a period of 180 Days. Fig. 16 illustrates the 3D plot of the fluorescence spectra of the CQDs for day 1 and day 180. Based on Fig. 16, it was found that even after 180 days, the synthesized CQDs still exhibited almost similar fluorescence results to Day 1. This shows that the synthesized CQDs exhibit long-term stability, which is favourable for various long-term applications, including water quality control. Furthermore, based on the results obtained from 3-D Measurement, the quantum yield percentage of the CQDs after 180 days was found to be 2.010% in comparison to 2.101% on Day 1. This further proves the strong stability of the synthesized CQDs.

Measurement of the antibacterial activity of CQDs

The antibacterial activity of the N–S doped CQDs was explored on *E. coli* (Gram-negative). Equal amounts of bacteria were treated with 400 mg mL^{-1} CQDs. Tetracycline was also used as the conventional antibiotic sample to compare the effectiveness of the CQDs in inhibiting the growth of the bacteria. A negative sample (with bacteria only) was included to clearly show the inhibitory effects of CQDs and tetracycline towards the bacteria. The inhibitory effects of the CQDs were quantitatively estimated in determining the effect of the MIC of CQDs on the bacterial growth. The bacterial viability was analysed by measuring the OD values of the bacterial mixture. The MIC results for *E. coli* are presented in Fig. 17. It was found that at the 48th hour, both CQD and tetracycline showed inhibition towards *E. coli*, where 400 mg mL^{-1} showed the highest inhibition towards *E. coli*.

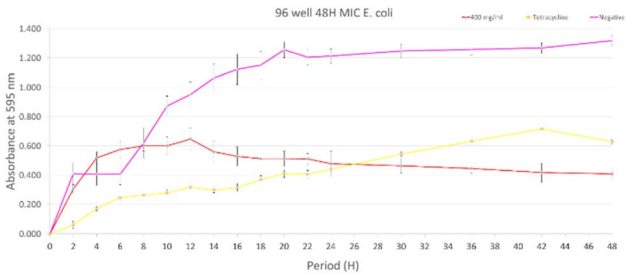

Fig. 17 48 hours 96 well MIC test for *E. coli* treated with both tetracycline and 400 mg mL^{-1} CQDs.

Compared to tetracycline, 400 mg mL^{-1} CQDs showed longer-lasting inhibition, especially from the 26th hour onwards. This is because tetracycline degraded over time due to heat and UV. Similar to some conventional antibiotics for wound healing, to supress the bacterial growth, medication ought to be applied 1 to 3 times daily.[85] Therefore, in comparison, it was shown that CQDs are more effective in bacterial growth inhibition for a long period of time, thus aiding in the commercialization of CQDs as a future alternative to antibiotics. In previous studies, N- or S-doped CQDs were reported to have little to zero inhibitory effects towards Gram-negative bacteria,[86] thus proving that the CQDs produced in this study had made a breakthrough in inhibiting Gram-negative bacteria.

To validate this finding, using different concentrations of CQD, the MIC test was again performed on 10, 50, 200, and 400 mg mL^{-1} CQDs. Tetracycline and a negative sample were also included for comparison. Fig. 18 shows the MIC results for this validation test. Based on Fig. 17 and 18, it was found that at the 48th hour, all concentrations used in the test showed inhibition towards *E. coli*. As seen in the figure, 200 mg mL^{-1} CQDs surpassed tetracycline at around the 40th hour. This proved that the CQDs could provide a longer inhibition time towards *E. coli*, especially at higher concentrations, in comparison to the conventional tetracycline.

To further test the theory of higher concentrations being equivalent to a greater antibacterial effect, 500 mg mL^{-1} of the CQD sample was applied to *E. coli,* and the MIC test was performed again. Results are presented in Fig. 19, which show that 500 mg mL^{-1} CQDs demonstrated an excellent inhibitory effect on *E. coli*. It was found that compared to 400 mg mL^{-1} (Fig. 17), the 500 mg mL^{-1} CQDs showed a better inhibitory effect than

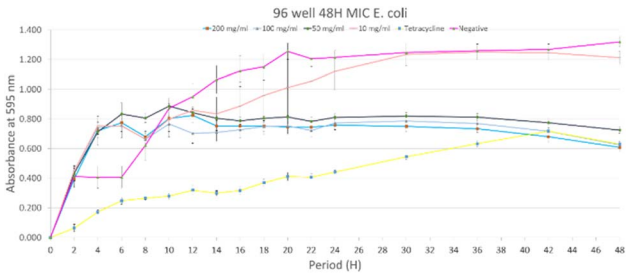

Fig. 18 48 hours 96 well MIC test for *E. coli* treated with both tetracycline and different concentrations of CQDs.

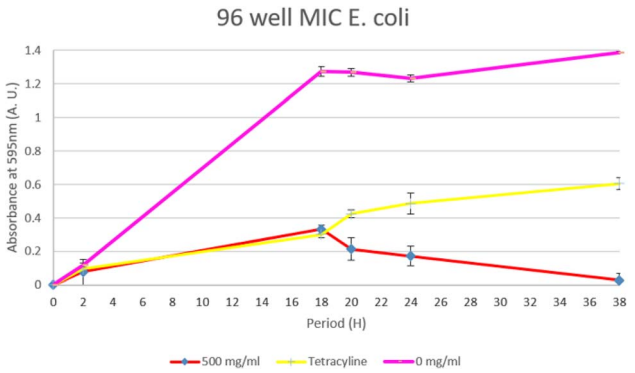

Fig. 19 38 hours 96 well MIC test for *E. coli* treated with both tetracycline and 500 mg mL^{-1} CQDs.

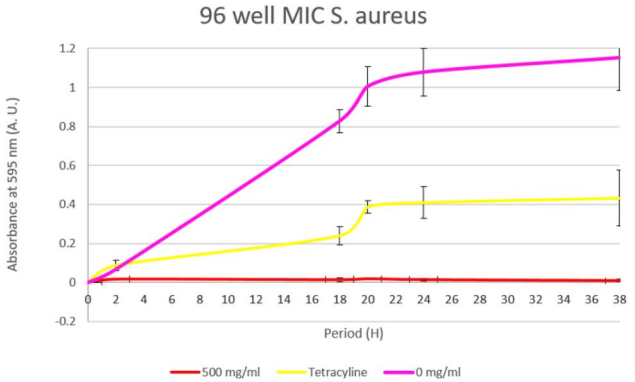

Fig. 20 38 hours 96 well MIC test for *S. aureus* treated with both tetracycline and 500 mg mL^{-1} CQDs.

tetracycline at around the 19th hour onwards, thus proving that the higher the CQD concentration, the higher the antibacterial effect exhibited by CQDs on *E. coli*, even better than the conventional tetracycline. Due to the outstanding antibacterial effect of CQDs towards *E. coli*, *S. aureus* (Gram-positive) was then tested using the MIC test. The results are shown in Fig. 20. According to Fig. 20, 500 mg mL^{-1} CQDs showed a significant inhibitory effect on *S. aureus* in comparison to *E. coli*. This might be due to the morphology of the bacteria. Unlike Gram-positive bacteria (*S. aureus*), Gram-negative bacteria (*E. coli*) contain an outer membrane, which is a barrier for antibiotics to pass through before accessing the target. Due to that outer membrane, Gram-negative bacteria are known to be more resistant to antibiotics than Gram-positive bacteria.[87] Based on the figure, CQDs have shown better antibacterial effect than tetracycline, thus proving that the CQDs are very effective against both *E. coli* and *S. aureus*, even exceeding the antibacterial efficiency of conventional tetracycline. Therefore, CQDs show great potential for commercialization as a green alternative antibiotic towards both Gram-positive and Gram-negative bacteria, due to their effective and long-lasting antibacterial properties.

Antibacterial mechanism of CQDs

To further verify the antibacterial effects of charged CQDs towards bacteria, zeta potential analysis was performed before

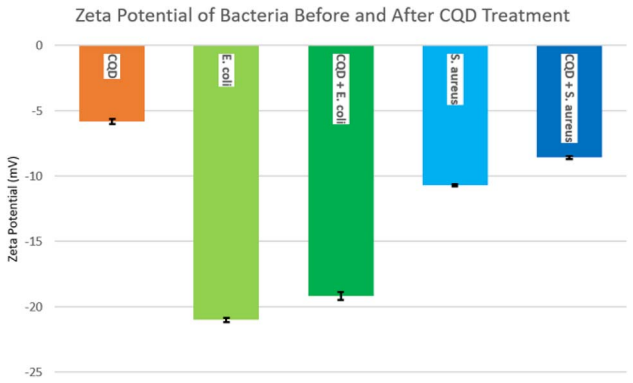

Fig. 21 Zeta potential of *E. coli* and *S. aureus* before and after CQD treatment.

and after mixing 4 mg of CQDs with the bacteria. The results are presented in Fig. 21. Based on the results, before mixing, the CQDs (−5.83 mV), *E. coli* (−21 mV), and *S. aureus* (−10.7 mV) were negatively charged. However, after CQD treatment, both *E. coli* and *S. aureus* showed lower negative zeta potentials of −19.2 mV and −8.57 mV, respectively. This indicated that the CQDs were likely bonded with the bacteria, thus resulting in the cell walls being broken, ultimately causing the death of the bacteria. In other words, the drop in the zeta potential was due to the destabilization of the bacterial wall, thus causing an antibacterial effect towards the bacteria. To study the relationship between the concentration of CQD and antibacterial effect towards the bacteria, the zeta potentials of *E. coli* were then measured after being treated with two larger masses of CQDs, which were 25 mg and 50 mg, respectively. Fig. 22 shows the results of the test; after mixing with both 25 mg and 50 mg of CQDs, the zeta potential of *E. coli* dropped significantly to −11.07 mV and −6.94 mV, respectively. This indicates that the higher the concentration of CQDs, the less negative the zeta potential of *E. coli*, which also means the higher the antibacterial effect of the CQDs towards *E. coli*. This also corresponds to the MIC test, where the higher the CQD concentration, the stronger the inhibition was towards *E. coli*, as far as being more efficient than the conventional tetracycline.

Validation of antibacterial capabilities of CQDs

To further validate the antibacterial mechanism of CQDs, SEM was performed before and after treatment of the bacterium with CQDs. The SEM results are shown in Fig. 23 for *E. coli* and in Fig. 24 for *S. aureus*. After CQD treatment, *E. coli* has a much rougher surface with more wrinkles, while *S. aureus* shows a significant disruption of its shape. Based on these observations, it was concluded that both bacterial strains underwent cell lysis as a result of the damage induced by CQD treatment. These structural changes are highlighted with red circles. This proves that the N-CQDs had successfully influenced the morphology of both bacteria, especially *S. aureus.*

To verify the antibacterial mechanism of CQDs, an isotype test using the Kirby–Bauer disk diffusion method was carried out on both *S. ser. Typhimurium* and *V. parahaemolyticus* strains. The results are shown in Fig. 25 and Table 4. Based on the

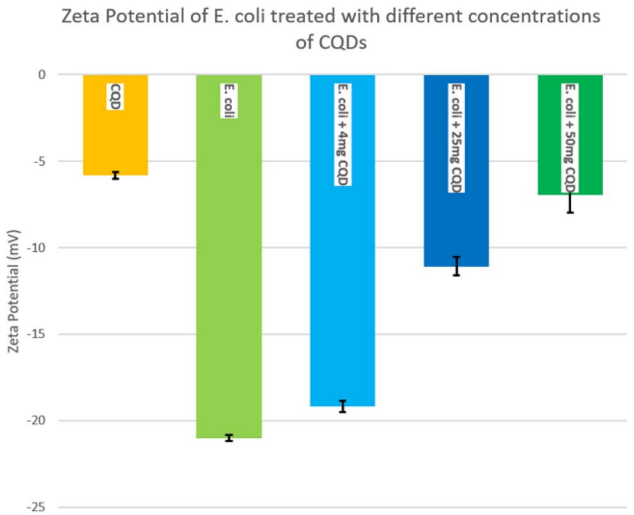

Fig. 22 Zeta potential of *E. coli* after treatment with different concentrations of CQDs.

results in Table 4, a significant zone of inhibition was found for both bacterial strains. This proves that the CQDs possess effective antibacterial mechanisms against different bacterial strains, namely, the four types of bacteria tested in this study. In addition, it was found that the higher the concentration, the larger the inhibition zone, and the stronger the antibacterial properties of the CQDs. The isotype test results also relate to the MIC analysis performed in the previous section for both *E. coli* and *S. aureus*, where CQDs at 500 mg mL^{-1} showed the best antibacterial properties compared to lower concentrations. The results of this study also prove that CQDs are a suitable candidate for a non-drug antibiotic due to their efficient antibacterial properties.

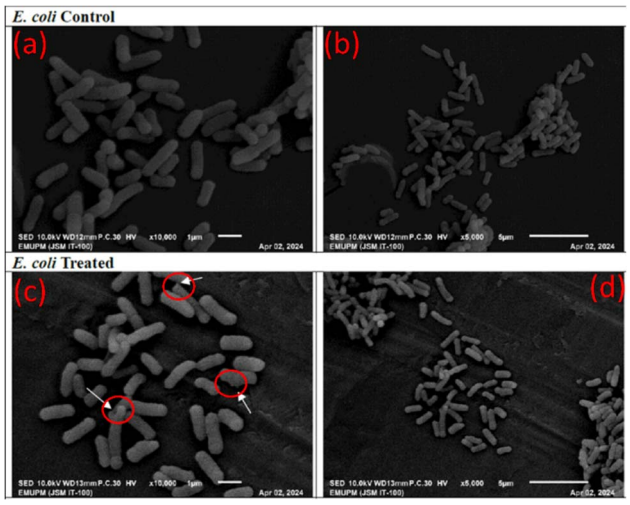

Fig. 23 SEM images of *E. coli*: (a) before CQD treatment at 10 000 magnification; (b) before CQD treatment at 5000 magnification; (c) after CQD treatment at 10 000 magnification; and (d) after CQD treatment at 5000 magnification.

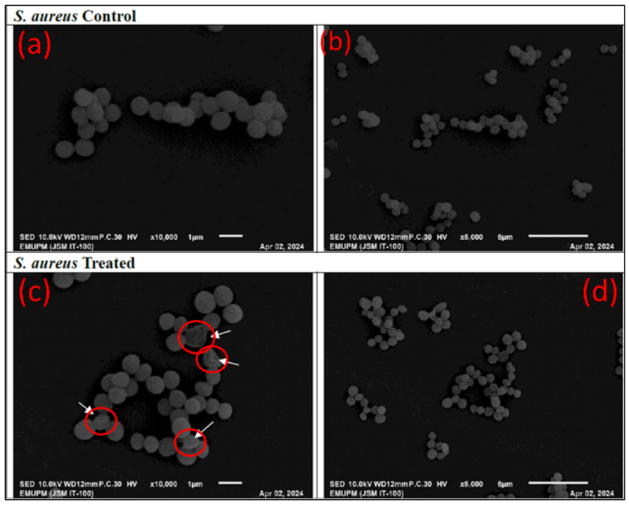

Fig. 24 SEM images of *S. aureus*: (a) before CQD treatment at 10 000 magnification; (b) before CQD treatment at 5000 magnification; (c) after CQD treatment at 10 000 magnification; and (d) after CQD treatment at 5000 magnification.

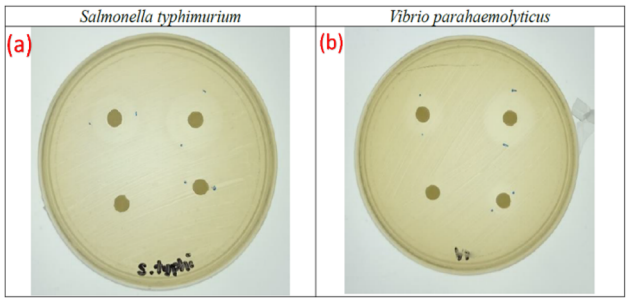

Fig. 25 Photos of disk diffusion plates containing (a) *S. ser. Typhimurium* and (b) *V. parahaemolyticus* taken after 8 hours of incubation with CQDs.

Table 4 Measurement of the inhibition zone at different CQD concentrations for *Salmonella typhimurium* and *Vibrio parahaemolyticus*

	Concentration		
Bacteria strain	500 mg mL^{-1}	250 mg mL^{-1}	125 mg mL^{-1}
Salmonella typhimurium	2.0 cm	1.7 cm	1.1 cm
Vibrio parahaemolyticus	2.0 cm	1.5 cm	1.0 cm

Strength of the current study

Table 5 shows the conditions and results of the natural CQDs synthesized from previous studies.[22,29–32,82,88–93] Comparing the CQDs synthesized in this study with those prepared in previous studies, as shown in Table 5, in terms of quantum yield percentage, it was found that the yield of the CQDs in the current study is significantly lower. The difference in quantum yield percentage may be due to the solvents used to prepare the CQDs. No solvent was used in this study, while in previous

Table 5 Summary of methods, conditions and results of the synthesis of CQDs from natural resources

					Results				
Precursors	Solvents	Temperature (°C)/ wattage (W)	Synthesis time (hr)	Method	Excitation (nm)	Emission (nm)	Quantum yield percentage (%)	Average size (nm)	Colour	References
Onion and sugar	—	850 W	0.05	Microwave irradiation	470	541.5	2.101	4–6	Green	Current study
Onion	Ethylenediamine (EDA)	120 °C	2	Hydrothermal	380	464	28	15	Blue	22
Lemon	Ethanol	120 °C	3	Hydrothermal	410	482	16.7	3.1	Blue	29
Lemon and onion	Deionized water and ammonium hydroxide	370 °C	0.1	Microwave Pyrolysis	340	425	23.6	6.15	Violet	30
Orange	Ethylenediamine (EDA)	120 °C	2.5	Hydrothermal	370	452	26	1.5–4.5	Blue	31
Carrot juice	Ultrapure water	160 °C	6	Hydrothermal	360	442	5.16	5.5	Blue	82
Pulp-free lemon juice	Formamide	200 °C	6	Hydrothermal	605	704	31	5.7	Red	88
Ziziphus mauritiana seeds	Ethanol	150 W	0.33 (20 min)	Microwave Pyrolysis	375	475	14.6	2–4	Blue	89
Orange juice	Urea	2800 W	0.17 (10 min)	Microwave Pyrolysis	325	417	29.3	2–5	Violet	90
P. acidus fruit	Aqueous ammonia	180 °C	8	Hydrothermal	350	420	14	3.5–5.5	—	91
Dwarf banana peel	Aqueous ammonia	200 °C	24	Hydrothermal	345	413	23	2.5–5.5	Blue	92
Kiwi fruit peel	Aqueous ammonia	200 °C	24	Hydrothermal	360	425	18	3–7	Blue	93
Lemon and onion	—	120 °C	3	Hydrothermal	485	566	1.35	—	Green	32

studies, solvents such as ethylenediamine (EDA), ethanol, and ammonium hydroxide were used to significantly enhance the performance of the CQDs. Solvents could aid in the increase of quantum yield percentage, as well as affect the length of increase of its polarity and viscosity.[94] Despite the low quantum yield percentage exhibited, the CQDs synthesized in this research are consumer-friendly due to the preparation materials being non-toxic and all-natural. This is beneficial towards the aim of being the future green alternative for drug-based antibiotics against the emerging drug-resistant bacteria, as they could be safely consumed or applied without the fear of toxicity or side effects. Furthermore, unlike some of the previous studies, the excitation peak wavelength of the CQDs synthesized in this study is in the visible light region, which means that visible light could be used to excite the CQDs for the highest efficiency. Therefore, the CQDs prepared in this study are safe for *in vivo* applications, such as bioimaging and nanomedicines. Moreover, the CQDs prepared in this study exhibit promising antibacterial properties towards both Gram-positive (*S. aureus*) and Gram-negative (*E. coli*) bacteria. In comparison to the conventional antibiotic, tetracycline, CQDs from this study show fast antibacterial effectiveness and longer-lasting effects towards both types of bacteria, especially at an optimal concentration of 500 mg mL^{-1}. This proves that the CQDs synthesized in this study have high potential in acting as a green alternative towards the ever-challenging drug-resistant bacteria.

Additionally, the CQDs produced in this study require a low cost to synthesize, and the synthesis process is simple and fast. The materials that were used to synthesize CQDs in this study are natural resources, including onions and sugar. Hence, the cost of materials is relatively lower in comparison to drug-based antibiotics. On the other hand, the synthesis process is very effortless *via* the microwave irradiation method and only requires 3 minutes of heating. The fast and simple synthesis of the CQDs is very favourable towards large-scale industries as it vastly reduces the production cost and manpower, thus aiding in the commercialization of the CQDs as the future green antibiotic alternative.

Conclusion

Using onions as the precursor, fluorescent CQDs have been successfully synthesized *via* the hydrothermal method. The results show that a quantum yield of 0.223% was exhibited by the synthesized CQDs. Parameters were investigated to enhance the performance of the CQDs prepared, such as the CQD synthesis method, the addition of other materials, the ratio of the mixture, the volume of the preparation mixture, and the pH of the CQD solution. It was concluded that the optimal conditions for the synthesis of the CQDs are as follows: mixing with sugar at an onion-sugar ratio of 3 : 7, the microwave irradiation method, 250 mL, and a pH of 7–8. CQDs that were synthesized based on the optimal conditions produced a quantum yield of 2.101%, which is 9.4 times higher than the quantum yield percentage of the initial onion CQDs. Although the quantum yield percentage is lower in comparison to chemical-based CQDs from previous studies, the CQDs synthesized in this study are chemical-free and

could perform optimally under visible light excitation, thus proving that they could be safely used for *in vivo* applications, such as bioimaging and nanomedicines. In addition, the CQDs in this study require a shorter synthesis time, thus making them favourable for industrial commercialization purposes. Moreover, the surfaces of the synthesized CQDs were found to be functionalized with both nitrogen and sulphur-containing functional groups, thus verifying that N–S-CQDs were successfully produced using natural resources. While most N–S-CQDs produced from previous studies used harsh chemicals as precursors and solvents, in this study, only soft commodities are required for the synthesis. This is important as it proves that the functionalization of the CQDs does not necessarily require the participation of chemicals. Based on the characterizations, the products synthesized in this study are N,S-CQDs, which satisfy the conditions of being fluorescent, amorphous, and smaller than 10 nm, as well as containing nitrogen and sulphur surface functional groups. Moreover, as a means to commercialize CQDs as a green alternative to antibiotics towards the emerging drug-resistant bacteria, the synthesized CQDs were tested against both Gram-negative (*E. coli*) and Gram-positive (*S. aureus*) bacteria for their antibacterial effectiveness. Based on the MIC test, compared to tetracycline, 500 mg mL^{-1} CQDs have shown immediate and longer-lasting results towards both *E. coli* and *S. aureus*. The success of this research could lead to a variety of contributions to society and the economy. On the society side, it is important for the synthesis materials to be non-toxic and that zero chemicals are added so that the synthesized CQD are also non-toxic. Both the CQD synthesis routes studied do not involve any addition of chemicals or toxic materials; thus, the synthesized CQDs are of zero toxicity. In addition, the by-products after synthesis are biodegradable; thus, no long-lasting waste is produced. On the economic side, being non-toxic, these CQDs could be used to replace the conventional wound healing medications. Consumers will feel more at ease using the medications, knowing that they will not be harmed by the non-toxic CQDs. Hence, the nature-based N,S-CQDs synthesized in this study show great potential for the commercialization of green and consumer-safe antibiotics. However, further antibacterial studies would be highly beneficial on the road to commercialization.

Conflicts of interest

The authors declare that they have no known competing financial interests or personal relationships that could have appeared to influence the work reported in this paper.

Data availability

The data that support the findings of this study are available from the corresponding author upon reasonable request.

Acknowledgements

The authors are grateful to the Fundamental Research Grant Scheme (FRGS/1/2021/STG05/XMU/02/2) from the Ministry of Higher Education Malaysia and Xiamen University Malaysia Research Fund (XMUMRF/2024-C13/IENG/0066) from Xiamen University Malaysia for financially supporting this work.

Notes and references

1 M. S. Morehead and C. Scarbrough, *Primary Care*, 2018, **45**, 467–484.
2 S. B. Singh, K. Young and L. L. Silver, *Biochem. Pharmacol.*, 2017, **133**, 63–73.
3 L. Poirel, J. Y. Madec, A. Lupo, A. K. Schink, N. Kieffer, P. Nordmann and S. Schwarz, *Microbiol. Spectrum*, 2018, **6**, 1–26.
4 B. Mlynarczyk-Bonikowska, C. Kowalewski, A. Krolak-Ulinska and W. Marusza, *Int. J. Mol. Sci.*, 2022, **23**, 8088–8121.
5 S. Chernousova and M. Epple, *Angew Chem. Int. Ed. Engl.*, 2013, **52**, 1636–1653.
6 C. Cao, W. Ge, J. Yin, D. Yang, W. Wang, X. Song, Y. Hu, J. Yin and X. Dong, *Small*, 2020, **16**, e2000436.
7 Y. Xie, J. Yang, J. Zhang, W. Zheng and X. Jiang, *Angew Chem. Int. Ed. Engl.*, 2020, **59**, 23471–23475.
8 C. Weng, L. Shen and W. H. Ang, *Angew Chem. Int. Ed. Engl.*, 2020, **59**, 9314–9318.
9 T. Deng, H. Zhao, M. Shi, Y. Qiu, S. Jiang, X. Yang, Y. Zhao and Y. Zhang, *Small*, 2019, **15**, e1902647.
10 X. Xie, T. Sun, J. Xue, Z. Miao, X. Yan, W. Fang, Q. Li, R. Tang, Y. Lu, L. Tang, Z. Zha and T. He, *Adv. Funct. Mater.*, 2020, **30**, 2000511.
11 Y. Zhou, Y. Guo, J. Li, W. Wei, D. Li, L. Luo, X. Xu and Z. Zhou, *J. Mater. Chem. A*, 2020, **8**, 11511–11514.
12 R. Wang, M. Shi, F. Xu, Y. Qiu, P. Zhang, K. Shen, Q. Zhao, J. Yu and Y. Zhang, *Nat. Commun.*, 2020, **11**, 4465.
13 X. Li, M. Liang, S. Jiang, S. Cao, S. Li, Y. Gao, J. Liu, Q. Bai, N. Sui and Z. Zhu, *ACS Appl. Mater. Interfaces*, 2021, **13**, 22169–22181.
14 P. Li, S. Liu, X. Yang, S. Du, W. Tang, W. Cao, J. Zhou, X. Gong and X. Xing, *Chem. Eng. J.*, 2021, **403**, 126387.
15 S. Liu, T. H. Zeng, M. Hofmann, E. Burcombe, J. Wei, R. Jiang, J. Kong and Y. Chen, *ACS Nano*, 2011, **5**, 6971–6980.
16 M. J. Molaei, *Anal. Methods*, 2020, **12**, 1266–1287.
17 L. Tang, R. Ji, X. Cao, J. Lin, H. Jiang, X. Li, K. S. Teng, C. M. Luk, S. Zeng, J. Hao and S. P. Lau, *ACS Nano*, 2012, **6**, 5102–5110.
18 B. D. Mansuriya and Z. Altintas, *Nanomaterials*, 2021, **11**, 2525.
19 P. Zuo, X. Lu, Z. Sun, Y. Guo and H. He, *Microchim. Acta*, 2016, **183**, 519–542.
20 F. Yuan, S. Li, Z. Fan, X. Meng, L. Fan and S. Yang, *Nano Today*, 2016, **11**, 565–586.
21 M. J. Molaei, *Sol. Energy*, 2020, **196**, 549–566.
22 R. Bandi, B. R. Gangapuram, R. Dadigala, R. Eslavath, S. S. Singh and V. Guttena, *RSC Adv.*, 2016, **6**, 28633–28639.
23 Q. Xu, Q. Zhou, Z. Hua, Q. Xue, C. Zhang, X. Wang, D. Pan and M. Xiao, *ACS Nano*, 2013, **7**, 10654–10661.
24 M. Shamsipur, A. Barati, A. A. Taherpour and M. Jamshidi, *J. Phys. Chem. Lett.*, 2018, **9**, 4189–4198.

25 J. Ren, F. Weber, F. Weigert, Y. Wang, S. Choudhury, J. Xiao, I. Lauermann, U. Resch-Genger, A. Bande and T. Petit, *Nanoscale*, 2019, **11**, 2056–2064.
26 P. G. Luo, S. Sahu, S.-T. Yang, S. K. Sonkar, J. Wang, H. Wang, G. E. LeCroy, L. Cao and Y.-P. Sun, *J. Mater. Chem. B*, 2013, **1**, 2116–2127.
27 K. J. Mintz, Y. Zhou and R. M. Leblanc, *Nanoscale*, 2019, **11**, 4634–4652.
28 S. Wang, I. S. Cole, D. Zhao and Q. Li, *Nanoscale*, 2016, **8**, 7449–7458.
29 S. S. Monte-Filho, S. I. E. Andrade, M. B. Lima and M. C. U. Araujo, *J. Pharm. Anal.*, 2019, **9**, 209–216.
30 M. He, J. Zhang, H. Wang, Y. Kong, Y. Xiao and W. Xu, *Nanoscale Res. Lett.*, 2018, **13**, 175.
31 D. Kumar, K. Singh, V. Verma and H. Bhatti, *J. Bionanosci.*, 2014, **8**, 274–279.
32 Y. Khor, A. R. Abdul Aziz and S. S. Chong, *Int. J. Nanoelectron. Mater.*, 2022, **15**, 241–253.
33 W. Lu, X. Gong, M. Nan, Y. Liu, S. Shuang and C. Dong, *Anal. Chim. Acta*, 2015, **898**, 116–127.
34 Y.-P. Sun, X. Wang, F. Lu, L. Cao, M. J. Meziani, P. G. Luo, L. Gu and L. M. Veca, *J. Phys. Chem. C*, 2008, **112**, 18295–18298.
35 J. Liang, Y. Jiao, M. Jaroniec and S. Z. Qiao, *Angew. Chem., Int. Ed.*, 2012, **51**, 11496–11500.
36 J. Manioudakis, F. Victoria, C. A. Thompson, L. Brown, M. Movsum, R. Lucifero and R. Naccache, *J. Mater. Chem. C*, 2019, **7**, 853–862.
37 J. Duan, J. Yu, S. Feng and L. Su, *Talanta*, 2016, **153**, 332–339.
38 N. A. Travlou, D. A. Giannakoudakis, M. Algarra, A. M. Labella, E. Rodríguez-Castellón and T. J. Bandosz, *Carbon*, 2018, **135**, 104–111.
39 G. Yang, X. Wan, Y. Su, X. Zeng and J. Tang, *J. Mater. Chem. A*, 2016, **4**, 12841–12849.
40 S. Chai, L. Zhou, S. Pei, Z. Zhu and B. Chen, *Micromachines*, 2021, **12**, 1116.
41 S. K. Tammina, D. Yang, S. Koppala, C. Cheng and Y. Yang, *J. Photochem. Photobiol., B*, 2019, **194**, 61–70.
42 A. K. Roy, S.-M. Kim, P. Paoprasert, S.-Y. Park and I. In, *RSC Adv.*, 2015, **5**, 31677–31682.
43 S. Pandiyan, L. Arumugam, S. P. Srirengan, R. Pitchan, P. Sevugan, K. Kannan, G. Pitchan, T. A. Hegde and V. Gandhirajan, *ACS Omega*, 2020, **5**, 30363–30372.
44 M. Budimir, Z. Marković, J. Vajdak, S. Jovanović, P. Kubat, P. Humpoličček, M. Mičušik, M. Danko, A. Barras, D. Milivojević, Z. Špitalsky, R. Boukherroub and B. T. Marković, *Radiat. Phys. Chem.*, 2021, **185**, 109499.
45 M. Tariq, A. Singh, N. Varshney, S. K. Samanta and M. P. Sk, *Mater. Today Commun.*, 2022, **33**, 104347.
46 M. Tariq, S. Shivalkar, H. Hasan, A. K. Sahoo and M. P. Sk, *ACS Omega*, 2023, **8**, 49460–49466.
47 M. Tariq, M. A. Khan, H. Hasan, S. Yadav, A. K. Sahoo and M. P. Sk, *RSC Sustain.*, 2024, **2**, 3114–3122.
48 M. Tim, *J. Photochem. Photobiol., B*, 2015, **150**, 2–10.
49 S. Yougbaré, C. Mutalik, D. I. Krisnawati, H. Kristanto, A. Jazidie, M. Nuh, T. M. Cheng and T. R. Kuo, *Nanomaterials*, 2020, **10**, 1123.
50 R. Knoblauch and C. D. Geddes, *Materials*, 2020, **13**, 4004.
51 S. Gao, X. Yan, G. Xie, M. Zhu, X. Ju, P. J. Stang, Y. Tian and Z. Niu, *Proc. Natl. Acad. Sci. U. S. A.*, 2019, **116**, 23437–23443.
52 Y. Chen, Y. Gao, Y. Chen, L. Liu, A. Mo and Q. Peng, *J. Controlled Release*, 2020, **328**, 251–262.
53 X. Dong, L. Ge, D. I. Abu Rabe, O. O. Mohammed, P. Wang, Y. Tang, S. Kathariou, L. Yang and Y.-P. Sun, *Carbon*, 2020, **170**, 137–145.
54 J. M. V. Makabenta, A. Nabawy, C. H. Li, S. Schmidt-Malan, R. Patel and V. M. Rotello, *Nat. Rev. Microbiol.*, 2021, **19**, 23–36.
55 S. Y. Lim, W. Shen and Z. Gao, *Chem. Soc. Rev.*, 2015, **44**, 362–381.
56 L. Liguori, R. Califano, D. Albanese, F. Raimo, A. Crescitelli and M. Di Matteo, *J. Food Qual.*, 2017, **2017**, 6873651.
57 G. He, M. Xu, M. Shu, X. Li, Z. Yang, L. Zhang, Y. Su, N. Hu and Y. Zhang, *Nanotechnology*, 2016, **27**, 395706.
58 D. Bano, S. Chandra, P. Yadav, V. K. Singh and S. Hasan, *J. Photochem. Photobiol., A*, 2020, **398**, 112558.
59 N. Locquet, A. Aït-Kaddour and C. B. Y. Cordella, in *Encyclopedia of Analytical Chemistry*, 2018, DOI: **10.1002/9780470027318.a9540**, pp. 1–39.
60 F. A. Villamena, in *Reactive Species Detection in Biology*, ed. F. A. Villamena, Elsevier, Boston, 2017, pp. 87–162, DOI: **10.1016/B978-0-12-420017-3.00003-7**.
61 D. Titus, E. James Jebaseelan Samuel and S. M. Roopan, in *Green Synthesis, Characterization and Applications of Nanoparticles*, ed. A. K. Shukla and S. Iravani, Elsevier, 2019, pp. 303–319, DOI: **10.1016/B978-0-08-102579-6.00012-5**.
62 M. A. O'Keefe, P. R. Buseck and S. Iijima, *Nature*, 1978, **274**, 322–324.
63 M. Joshi and A. Bhattacharyya, *Indian J. Fibre Text. Res.*, 2008, **33**, 304–317.
64 R. A. Pethrick and C. Viney, *Techniques for Polymer Organisation and Morphology Characterisation*, Wiley, 2003.
65 R. W. Richards, *Scattering Methods in Polymer Science*, Ellis Horwood, 1995.
66 J. Bergström, in *Mechanics of Solid Polymers*, ed. J. Bergström, William Andrew Publishing, 2015, DOI: **10.1016/B978-0-323-31150-2.00002-9**, pp. 19–114.
67 L. Nicholas, *Infrared Spectroscopy*, 2020, **https://chem.libretexts.org/Bookshelves/Physical_and_Theoretical_Chemistry_Textbook_Maps/Supplemental_Modules_(Physical_and_Theoretical_Chemistry)/Spectroscopy/Vibrational_Spectroscopy/Infrared_Spectroscopy**, accessed 25 November 2023.
68 J. Mathias, *How Does FTIR Work?*, 2015, **https://www.innovatechlabs.com/newsroom/672/stuff-works-ftir-analysis/**, accessed 25 November 2023.
69 Sigma-Aldrich, *IR Spectrum Table & Chart*, 2015, **https://www.sigmaaldrich.com/technical-documents/articles/biology/ir-spectrum-table.html**, accessed 25 November 2023.
70 B. Kowalska-Krochmal and R. Dudek-Wicher, *Pathogens*, 2021, **10**, 165.

71 A. P. V. Ferreyra Maillard, J. C. Espeche, P. Maturana, A. C. Cutro and A. Hollmann, *Biochim. Biophys. Acta, Biomembr.*, 2021, **1863**, 183597.
72 Y. R. Herrero, K. L. Camas and A. Ullah, in Advanced Applications of Biobased Materials, ed. S. Ahmed and Annu, Elsevier, 2023, DOI: **10.1016/B978-0-323-91677-6.00005-2**, pp. 111–143.
73 B. J. Inkson, in *Materials Characterization Using Nondestructive Evaluation (NDE) Methods*, ed. G. Hübschen, I. Altpeter, R. Tschuncky and H.-G. Herrmann, Woodhead Publishing, 2016, pp. 17–43, DOI: **10.1016/B978-0-08-100040-3.00002-X**.
74 X. Zhu, Q. Su, W. Feng and F. Li, *Chem. Soc. Rev.*, 2017, **46**, 1025–1039.
75 C. Yang, J. Zhang, W.-T. Peng, W. Sheng, D. Liu, P. S. Kuttipillai, M. Young, M. R. Donahue, B. G. Levine, B. Borhan and R. R. Lunt, *Sci. Rep.*, 2018, **8**, 16359.
76 Z. Fatahi, N. Esfandiari, H. Ehtesabi, Z. Bagheri, H. Tavana, Z. Ranjbar and H. Latifi, *EXCLI J.*, 2019, **18**, 454–466.
77 N. Yadav, A. Sharma, T.-a. Yano, T. D. Anthopoulos and V. Mishra, *Coord. Chem. Rev.*, 2026, **548**, 217152.
78 A. Vibhute, T. Patil, R. Gambhir and A. P. Tiwari, *Appl. Surf. Sci. Adv.*, 2022, **11**, 100311.
79 T. L. Oliveira and A. K. Alves, in *Technological Applications of Nanomaterials*, ed. A. Kopp Alves, Springer International Publishing, Cham, 2022, pp. 71–88, DOI: **10.1007/978-3-030-86901-4_4**.
80 A. B. Siddique, A. K. Pramanick, S. Chatterjee and M. Ray, *Sci. Rep.*, 2018, **8**, 9770.
81 L. Cao, M. J. Meziani, S. Sahu and Y.-P. Sun, *Acc. Chem. Res.*, 2013, **46**, 171–180.
82 Y. Liu, Y. Liu, M. Park, S.-J. Park, Y. Zhang, M. Akanda, B.-Y. Park and H. Kim, *Carbon Lett.*, 2017, **21**, 61–67.
83 X. Han, J. Lei, K. Chen, Q. Li, H. Hao, T. Zhou, F.-L. Jiang, M. Li and Y. Liu, *Ecotoxicol. Environ. Saf.*, 2019, **174**, 467–474.
84 Z. Fakhroueian, R. Vahabpour, M. Assmar, A. Massiha, A. Zahedi, P. Esmaeilzadeh, F. Katouzian, S. Rezaei, P. Keyhanvar and A. Mozafari Dehshiri, *Artif. Cells, Nanomed., Biotechnol.*, 2018, **46**, 96–111.
85 N. S. Trookman, R. L. Rizer and T. Weber, *J. Am. Acad. Dermatol.*, 2011, **64**, S8–S15.
86 Q. Dou, X. Fang, S. Jiang, P. L. Chee, T.-C. Lee and X. J. Loh, *RSC Adv.*, 2015, **5**, 46817–46822.
87 Z. Breijyeh, B. Jubeh and R. Karaman, *Molecules*, 2020, **25**, 1340.
88 H. Ding, X. Zhou, B. Qin, Z. Zhou and Y. Zhao, *J. Lumin.*, 2019, **211**, 298–304.
89 S. Ganesan, R. Kalimuthu, T. Kanagaraj, R. Kulandaivelu, R. Nagappan, L. A. Pragasan and V. K. Ponnusamy, *Environ. Res.*, 2022, **206**, 112589.
90 G. Magdy, F. Belal and H. Elmansi, *RSC Adv.*, 2023, **13**, 4156–4167.
91 R. Atchudan, T. Edison, K. R. Aseer, S. Perumal, N. Karthik and Y. R. Lee, *Biosens. Bioelectron.*, 2018, **99**, 303–311.
92 R. Atchudan, T. N. J. I. Edison, S. Perumal, N. Muthuchamy and Y. R. Lee, *Fuel*, 2020, **275**, 117821.
93 R. Atchudan, S. Chandra Kishore, P. Gangadaran, T. N. Jebakumar Immanuel Edison, S. Perumal, R. L. Rajendran, M. Alagan, S. Al-Rashed, B.-C. Ahn and Y. R. Lee, *Environ. Res.*, 2022, **204**, 112365.
94 *Principles of Fluorescence Spectroscopy*, ed. J. R. Lakowicz, Springer US, Boston, MA, 2006, pp. 205–235, DOI: **10.1007/978-0-387-46312-4_6**.